



## Research papers

# Precipitation-based climate change hotspots across India through a Multi-model assessment from CMIP6

Subharthi Sarkar, Subhra Sekhar Maity, Rajib Maity\*

Department of Civil Engineering, Indian Institute of Technology Kharagpur, Kharagpur 721302, West Bengal, India



## ARTICLE INFO

## Keywords:

Climate Change Hotspots  
Precipitation Extremes  
Precipitation-based Hotspot Index (PHI)  
Precipitation-based Vulnerability Index (PVI)  
Homogeneous Precipitation Zones (HPZs)  
Coupled Model Intercomparison Project version 6 (CMIP6)

## ABSTRACT

This study presents an analysis to identify precipitation-based climate change hotspots and key-vulnerable cities using multi-model, multi-scenario, high-resolution ( $0.25^\circ \times 0.25^\circ$ ), bias-corrected precipitation dataset across India from 14 state-of-the-art General Circulation Models (GCMs), participating in Coupled Model Intercomparison Project version 6 (CMIP6). Preliminary analysis indicates an overall wetter future across India with  $290 \pm 150$  mm to  $530 \pm 260$  mm increase in mean annual precipitation towards end of this century under various climate change scenarios. Apart from the mean precipitation, the extremes are also found to be increasing by alarmingly higher rates. However, the spatio-temporal variations of such increments are notably diverse over different seasons in a year and across different Homogeneous Precipitation Zones (HPZs) in the country. Therefore, a new and more inclusive index, named as Precipitation-based Hotspot Index (PHI), is developed to identify the 'precipitation-based hotspots', i.e. the places with most pronounced changes in precipitation characteristics. The PHI considers the changes in various aspects of precipitation, such as mean, variability, and characteristics of extremes (magnitude, frequency and intensity). Based on the PHI values in the far-future period (2061–2100) and for the worst climate change scenario, the hotspot regions are identified mostly in the northwest, west-central, west coast, and northeast parts of India. Further, considering two important socio-economic vulnerability factors (population density and human development index) along with PHI, the key-vulnerable tier-I cities are identified across India. The analysis reveals four out of ten tier-I cities will be highly vulnerable towards end of this century. The findings of this analysis (hotspot maps) and the data products (high-resolution, bias-corrected precipitation dataset) are expected to be highly beneficial for impact assessments, hydrologic modelling, and formulating suitable adaptation and mitigation strategies for India over future.

## 1. Introduction

The observed changes in various natural systems on the Earth, such as atmosphere, oceans, land, cryosphere, and biosphere, since the pre-industrial era carries the unequivocal signature of anthropogenic climate change and its ever-increasing impacts (Flato et al., 2013). If the present rate of greenhouse gas emissions continues in the future as well, it will be highly unlikely to limit global warming to the internationally agreed-upon target (UNFCCC, 2015) of  $2^\circ\text{C}$  above the pre-industrial baseline (Knutti et al., 2016; Roe et al., 2019; Rogelj et al., 2016). However, how this global-scale warming will manifest at smaller spatial and temporal scales - remains a key question to the scientific community for understanding the changing pattern of climate, and hence for planning local- or national-scale adaptation and mitigation strategies. Therefore among this potential spatial heterogeneity in the climatic

responses, there exists a need to identify the 'climate change hotspots', i.e. the places with the strongest and most robust aggregated response to global-scale climatic forcing. Identification of such hotspots and their underlying mechanisms have been a topic of central interest in the Earth system research since many years now (Stocker et al., 2013). In particular, depicting such hotspots in a map format with strong visual elements, termed as 'hotspots map', is highly beneficial from academic, as well as policy-makers' point of view. Such hotspot mapping can communicate multiple key-information in an easier and user-friendly manner than a simple text document. Sometimes, along with the climatic exposure, the societal vulnerability is also included in identification of hotspots, which includes socio-economic status, sensitivity, coping capacity etc. of the concerned region (de Sherbinin, 2014). However, the quantitative estimates of these measures is always questionable, along with their lack of availability and reliability. Thus,

\* Corresponding author.

E-mail addresses: [rajib@civil.iitkgp.ac.in](mailto:rajib@civil.iitkgp.ac.in), [rajibmaity@gmail.com](mailto:rajibmaity@gmail.com) (R. Maity).

although the impacts of climate change are closely associated with societal vulnerability, identification of most responsive regions under changing climate is the primary and most crucial step in risk assessment and adaptation strategies.

Towards this, we have considered the entire Indian mainland as our study area. India, and South Asia as a whole, has been identified as one of the highly vulnerable regions under the changing climatic scenario owing to combination of various climatic and socio-economic factors, such as strong signals of climate change, high population density, low per capita income, developing economy etc. (De Souza et al., 2015; Mani et al., 2018). Consequently, enormous challenges are expected to be imposed on the agricultural productivity, water resources management, infrastructure, and livelihood of millions of people residing in this part of the globe, including India (Mishra et al., 2020). Therefore, development of hotspot maps for India as the preliminary step for adaptation and mitigation strategies will be decidedly required in near future to alleviate the detrimental effects of climate change and to help build resilience against the worst (Costello et al., 2009; De Souza et al., 2015). These hotspot maps can be developed for different climatic variables or phenomena which are predominantly affected by the changing climate such as temperature, precipitation, sea-level rise, cyclonic activities, etc. However, various recent incidents of floods and flash floods in different parts of India and their damaging impacts suggest a significant alteration in spatio-temporal pattern of precipitation across the country, for instance, the Coromandel Coast flood in 2015, East and West Godavari district flood in 2019, Kerala flood in 2018, 2019 and 2020, Assam flood in 2020, 2021, Bihar flood in 2019 etc. to name a few. On the other hand, studies report about 20–50% of the Indian mainland to be prone to moderate to extreme droughts (Suman and Maity, 2021) by the end of this century, with an increasing pattern in both intensity and areal extent (Mallya et al., 2016; Niranjan Kumar et al., 2013; Sharma and Mujumdar, 2017). Given such challenges, the changes in the regular spatio-temporal characteristics of precipitation are expected to have widespread implications on the overall availability of water resources and its management, thus, in turn affecting the food security of a country like India, whose economy primarily depends on rain-fed agriculture (Kishore et al., 2015). Hence, developing a precipitation-based hotspot map for India is indispensable, which sets the primary objective of this study.

India is a developing country with the second highest population in the world at present. Most of its cities are very ancient, ill-planned, and densely populated. Further, the inadequate drainage system in most of the cities is likely to cause water-stagnation and urban flooding under this future scenario of wet climate. Thus, crores of people living in those cities will face the nuisances created by urban flooding ranging from loss of property, disruption in transport and power supply to outbreak of epidemics and even deaths. Therefore, management of urban flooding and identification of such cities vulnerable to increased precipitation is also highly required – which sets another objective of this study.

Overall, such precipitation-based hotspot maps, as well as identification of key-vulnerable cities are expected to be immensely beneficial to combat future climate change-induced precipitation hazards in key-locations well in advance. However, to develop such precipitation-based hotspot map, an estimate of future-projected precipitation at a finer spatio-temporal scale is essential, which is mostly provided by General Circulation Models (GCMs). The GCMs are considered the most advanced tool for climate projection under different scenarios of greenhouse gas emissions, currently available worldwide (Flato et al., 2013). However, the spatial resolutions, at which GCMs run, are often too coarse to get reliable projections at the regional level for the impact assessment studies (Barbero et al., 2017; Kusumastuti et al., 2021; Maurer et al., 2010; Mishra et al., 2020). Moreover, the GCMs are found to produce precipitation output having significant amount of systematic bias due to their coarse resolution or model parameterizations (Ashfaq et al., 2017; Mishra et al., 2014), and thus, limiting their applicability to various research domains. Hence, bias-correction is a mandatory step

before using any GCM output, especially precipitation data (Mehrotra and Sharma, 2021; Sarkar and Maity, 2020a). Bias-correction methodologies have a long history in the literature (Kusumastuti et al., 2021; Li et al., 2010; Maraun, 2013; Mehrotra and Sharma, 2019, 2016; Vrac and Friederichs, 2015), including techniques, such as linear (Lenderink et al., 2007), non-linear (Leander et al., 2008; Leander and Buishand, 2007), distribution-based quantile mapping (Mao et al., 2015; Pierce et al., 2015), empirical quantile mapping (Piani et al., 2010; Themeßl et al., 2011), etc. However, most of the bias-correction methods suffer from one of the following two limitations: (a) they reduce bias in a selected precipitation quantile (e.g., either mean or extreme values) and (b) they exclude zero values from the analysis, even though their presence is significant in daily precipitation. Therefore, a recently developed copula-based bias-correction technique by Maity et al., (2019) (henceforth RMPH model) is used in this study, which de-biases the entire range of the precipitation- including the mean and different levels of extremes, and is particularly suitable for zero-inflated precipitation climatology like India. Comparing it with one of the most popular bias-correction methods, i.e., Quantile Mapping (QM) method, Suman et al., (2022) reported improved performance for both the mean and extreme precipitation values from the Coordinated Regional Climate Downscaling Experiment (CORDEX). Hence, the RMPH method is used in this study to correct the bias present in the precipitation output from GCMs. Nonetheless, we further compare the performance of RMPH and QM methods for the entire study area using GCM-simulated precipitation data from the latest version of Coupled Model Intercomparison Project, i.e., CMIP-6. Finally, the future-projected bias-corrected precipitation dataset for India using both RMPH and QM methods from multiple state-of-the-art CMIP-6 GCMs following various shared socio-economic pathways is made public by this study by keeping it in an open-source data repository (see 'Results and Discussion' section for details). We expect that this high-resolution, multi-model, multi-scenario dataset will be highly beneficial for different impact assessment studies over India.

Apart from just identification of hotspots, understanding their underlying mechanism is also very important. Towards this, we present a detailed and comprehensive spatio-temporal analysis on likely changes in various attributes of precipitation over future. Climatologically, the precipitation pattern across the Indian mainland varies significantly over space as well as time. Approximately 70% of the annual precipitation is received in four monsoon months (June through September) in India. The monsoon pattern is also different in different parts of the country, and is highly influenced by the steep topography of the Himalayas and the Western Ghats. Apart from the southwest monsoon, there is also the northeast monsoon, sometimes known as return monsoon that causes rainfall at some parts of India (mostly in the southern part of the country) during October to December. So, just an overall pan-India analysis of future changes in precipitation will not capture the complete picture of changing precipitation characteristics. Therefore, to conduct a holistic spatio-temporal analysis for India, we need to perform a spatio-temporal division as follows- (a) by dividing an entire year into some number of seasons and (b) by dividing the Indian mainland into some zones of spatially coherent precipitation pattern, namely Homogeneous Precipitation Zones or HPZs (See 'Methodology' section).

Thus, in brief, this study attempts to develop a future precipitation-based hotspot map across India based on multi-model multi-scenario bias-corrected precipitation dataset from CMIP-6. Based on this map, the vulnerability of all tier-I cities in India (with more than 1 lakh population as per census 2011) is also identified using various socio-economic factors. In general, the future precipitation-based hotspot maps, as well as the list of key-vulnerable cities will be highly beneficial not only for academic or research purposes, but for decision-making, risk analysis, impact assessments, and planning suitable adaptation and mitigation strategies. Additionally, this study publishes a multi-scenario, bias-corrected precipitation dataset from 14 state-of-the-art CMIP6-GCMs that

may be highly useful for other studies as well.

## 2. Data used

Different versions of CMIP, as established and monitored by the World Climate Research Programme (WCRP), provide a fundamental basis for a coordinated international climate research with an incredible technical contribution from several climate modelling centers (Eyring et al., 2016). Phase 6 of CMIP, i.e., CMIP6, is the most recent version that offers substantial improvements over its earlier versions in multiple aspects, such as finer horizontal resolution, better representation of the synoptic processes, and better agreement with the global energy balance (Supharatid et al., 2022). Thus, more reasonable and reliable projections can be obtained from CMIP6 outputs as compared to its previous versions (Chen et al., 2021; Di Luca et al., 2020; Li et al., 2021; Wang et al., 2021). We employ daily precipitation data from 14 state-of-the-art CMIP6-GCMs under r1i1p1f1 initial condition. Details of these models are shown in Table 1 (URL: <https://esgf-node.llnl.gov/search/cmip6/> accessed in December 2021). Total 80 years (2021–2100) of future data is obtained that is further divided into two equal parts, viz. near-future period (2021–2060) and far-future period (2061–2100), to capture the temporal changes in the precipitation characteristics w.r.t. the base period (1981–2010). Two different Shared Socioeconomic Pathways (SSPs), viz., SSP245 and SSP585, are considered for each GCM to understand two possible pathways of changes in the future. For instance, SSP585 is the most pessimistic scenario, i.e., SSP-5 with a target radiative forcing of  $8.5 \text{ W/m}^2$  by 2100 in a world with strong economic growth, abundant use of fossil fuel resources, rapid technological advances, but no suitable climate policy (Gidden et al., 2019). On the other hand, SSP245 depicts a ‘middle of the road’ scenario, i.e., SSP-2 with moderate population growth, uneven development and income growth across countries, and having a target radiative forcing of  $4.5 \text{ W/m}^2$  at the end of the century. Thus, comparison of results obtained between SSP585 and SSP245 will help us to understand the possible impact of higher anthropogenic activity and greenhouse gas emissions in the future.

The bias present in this GCM simulated dataset is corrected w.r.t. a gridded observational dataset, obtained from India Meteorological

**Table 1**  
Details of GCMs used in this study, participating in CMIP6.

Sl. No.	Model name	Horizontal resolution (latitude × longitude)	Source institute
1	ACCESS-CM2	$1.25^\circ \times 1.875^\circ$	Commonwealth Scientific and Industrial Research Organisation, Australia
2	ACCESS-ESM1-5	$1.25^\circ \times 1.875^\circ$	Beijing Climate Center, China
3	BCC-CSM2-MR	$1.1121^\circ \times 1.125^\circ$	Canadian Centre for Climate Modelling and Analysis, Canada
4	CanESM5	$2.7673^\circ \times 2.8125^\circ$	EC-Earth-Consortium
5	EC-Earth3	$0.70^\circ \times 0.70^\circ$	National Center for Atmospheric Research, USA
6	EC-Earth3-Veg	$0.70^\circ \times 0.70^\circ$	Fondazione Centro Euro-Mediterraneo sui Cambiamenti Climatici, Italy
7	CESM2_WACCM	$0.9424^\circ \times 1.25^\circ$	Max Planck Institute for Meteorology, Hamburg, Germany
8	CMCC-CM2-SR5	$0.9424^\circ \times 1.25^\circ$	Institut Pierre Simon Laplace, France
9	MPI-ESM1-2-HR	$0.935^\circ \times 0.9375^\circ$	Indian Institute of Tropical Meteorology Pune, India
10	MPI-ESM1-2-LR	$1.8652^\circ \times 1.8750^\circ$	Institute for Numerical Mathematics, Russian Academy of Science, Russia
11	IPSL-CM6A-LR	$1.2676^\circ \times 2.5^\circ$	
12	IITM	$1.9048^\circ \times 1.8750^\circ$	
13	INM-CM4-8	$1.5^\circ \times 2.0^\circ$	
14	INM-CM5-0	$1.5^\circ \times 2.0^\circ$	

Department (IMD). This  $0.25^\circ \times 0.25^\circ$  dataset was developed by Pai et al. (2014) using observed records of daily rainfall data from 6995 rain-gauge stations across India. This gridded precipitation dataset from IMD perfectly captures the precipitation climatology over India and has been successfully used for various hydroclimatic studies in recent times (Dash and Maity, 2019; Mishra et al., 2020; Mukherjee et al., 2018; Sarkar and Maity, 2020b).

## 3. Methodology

As per the set objectives of this study, the analysis is done in four stages. Firstly, the raw GCM precipitation data from all 14 models are re-gridded and bias-corrected. In the second stage, this bias-corrected multi-model multi-scenario dataset is undergone meticulous spatio-temporal analysis to understand the impact of changing climate on future precipitation. Next, the precipitation-based hotspot map is developed for the country, and finally, the most-vulnerable tier-I cities are identified across the country. The following sections explain the aforesaid steps in the methodology in detail.

### 3.1. Re-gridding and bias correction of future-simulated rainfall data from GCMs

The mismatch between spatial resolutions of 14 CMIP6-GCMs (Table 1) is taken care of by a standard re-gridding technique, namely bilinear interpolation, and all the datasets are re-gridded to a common resolution of  $0.25^\circ$  latitude  $\times$   $0.25^\circ$  longitude, same as that of IMD data.

Next, the RMPH method is adopted to correct the bias in GCM simulated precipitation values, as explained earlier (Maity et al., 2019; Suman et al., 2022). In this method, the concept of bivariate copula is used to model the association between observed (OBS) and historically simulated precipitation values (HSV) by developing a joint distribution function over a common historical time period (here, 1961–2014). Then, the conditional distribution function obtained from this joint distribution is modified as a mixed distribution with a discrete probability mass at zero to take care of the zero rainfall days. This is done by first dividing all the pairs of OBS and HSV into three groups: (i) pairs with both OBS and HSV having nonzero positive values, (ii) pairs with OBS = 0, and (iii) pairs with HSV = 0. Using these categorized pairs, primarily three sets of information are extracted while developing the RMPH model- (a) parameters for the best-fit copula model for the first set of pairs, (b) a suitable decay function capturing the probability for the second set, i.e., zero OBS conditioned on HSV over its entire range, and (c) conditional probability distribution of OBS values when HSV = 0, i.e., for the third set of pairs. Finally, by combining all this information, a set of conditional probability distribution of OBS values, given any value of HSV is obtained. These are used to obtain the bias-corrected precipitation values (BCV). Next, considering the future-simulated precipitation values as input (in place of HSV) to this set of conditional distribution function, bias-corrected precipitation values are obtained for future, and used for subsequent analysis. For further details about the RMPH method and its mathematical background, readers may refer to Maity et al. (2019).

Although the superiority of the RMPH method over the Quantile Mapping (QM) – another efficient and very popular bias correction technique, is already established in detail by Suman et al. (2022) for CMIP5-CORDEX simulations, we further compare their performance using the state-of-the-art CMIP6-GCMs. For applying the QM, the best-fit probability distributions are identified and fitted to both OBS and HSV over a common historical period. The selection of the best-fit marginal distribution is based on 12 candidate parametric probability distributions (e.g., beta, exponential, gamma, generalized pareto, inverse Gaussian, logistic, log logistic, lognormal, normal, Rayleigh, Rician, and Weibull) and two statistical criteria: (i) the fitted marginal distribution should pass the chi-square test at 5% significance level, and (ii) it should yield the lowest Bayesian information criterion (BIC).

### 3.2. Spatio-temporal analysis of future changes in precipitation

In order to perform a holistic analysis on future-projected changes over the diverse landscape of India, we perform a temporal decomposition, as well as a spatial decomposition. Temporally, we divide the entire year into four different seasons- (i) Summer (March-April-May), (ii) Monsoon (June-July-August-September), (iii) Post-monsoon (October-November-December), and (iv) Winter (January-February). Summer in India is mostly characterized by hot and dry weather with seldom occurrences of local-scale thunderstorms, followed by a four-month long monsoon season, with huge amount of rainfall (though spatially diverse) for most parts of the country due to humid south-westerly monsoon wind. During the post-monsoon season, a different monsoon cycle, the northeast (or “retreating”) monsoon, brings dry, cool, and dense air masses to large parts of India and causes heavy rainfall mostly in the southern part of the country (Tamilnadu and Kerala). Finally, the cold and dry winter season comes with very less amount of precipitation across the country.

Spatially also, we divide India into six different zones of spatially coherent precipitation characteristics, namely Homogeneous Precipitation Zones (HPZs) (Sarkar and Maity, 2022). This zoning is done by coupling two important features of precipitation- (i) average annual precipitation (P) and (ii) seasonal variation of monthly precipitation over the base period (1981–2010) using the observational records from IMD. The seasonality is quantified using an information theory-based metric named Apportionment Entropy (AE). Further details on this zoning can be found in the supplementary information (section A1). The HPZ map of India and its development from the scatter plot between P and AE are shown in Fig. 1. The originally obtained HPZ map in Fig. 1b is slightly modified in Fig. 1c with a hatched portion in the north-most part of the country (Jammu-Kashmir and Ladakh region). This portion is not considered in subsequent analysis in this study because of questionable

reliability of the IMD data in this region (Kothawale and Rajeevan, 2017). Detailed information on these six HPZs, their selection criterion, full name, abbreviation, etc. are listed in supplementary Table S1. Nevertheless, the HPZ-1 or ‘Low Precipitation-High Seasonality’ zone can be seen in the western part of India, predominantly consisting of Gujrat and Rajasthan. The HPZ-2 or ‘Moderate Precipitation-High Seasonality’ zone can be found in the central part of India, mostly spanning eastern Uttar Pradesh and Madhya Pradesh, and Chhattisgarh. The windward side of Western Ghats forms the HPZ-3 or ‘High Precipitation-High Seasonality zone’. The HPZ-4 or ‘Low Precipitation-Low Seasonality zone’ can be mainly observed in the Peninsular India. The HPZ-5 or ‘Moderate Precipitation-Low Seasonality zone’ is rather dispersed at multiple places across India; mostly in the eastern part of the country, parts of the eastern coast in Southern India, parts of Northern India (Uttarakhand and Himachal Pradesh) and some portion in North-east India as well. Lastly, the HPZ-6 or ‘High Precipitation-Low Seasonality zone’ can be mostly found in northeast India and Kerala.

Now, using this spatial and temporal decomposition, we perform three different sets of analysis. In the first set of analysis, the projected changes in seasonal precipitation are explored. The second set of analysis is designed to capture the changes in different levels of precipitation extremes over future. And, the likely changes in monthly variation of precipitation is examined in the third set of analysis. In the first and second set of analysis, the changes in different precipitation variables are expressed in terms of absolute changes (i.e., the changes in magnitude), and percentage changes w.r.t the base period (1981–2010). Additionally, a trend analysis is also performed to identify the places with statistically significant trend and its magnitude. The Mann-Kendall test at 5% significance level is performed to detect the significant trend, and Sen’s slope method (Sen, 1968) is used to evaluate the magnitude of the trend.

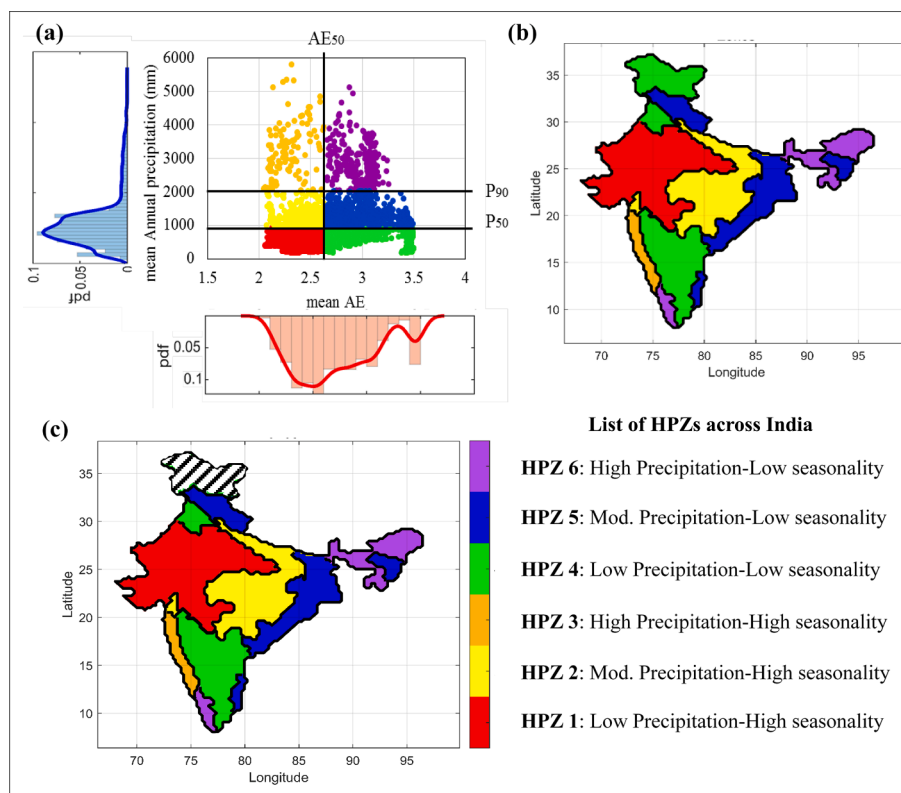


Fig. 1. Homogeneous Precipitation Zones (HPZs) across India. (a) Scatter plot between mean annual precipitation (P) and seasonality (AE) across India over the base period 1981–2010, and its delineation into six zones, (b) accordingly obtained HPZ map of India with six zones with different colours, and (c) modified HPZ map used in this study, with hatched portion in the north – not considered due to unreliable data quality.

Source: Sarkar and Maity, 2022

### 3.3. Identification of precipitation-based climate changes hotspots

Here, we use a climate response based approach to identify the 'precipitation-based climate changes hotspots' across India over future. In this approach, hotspot is defined as a region where climate variables (here, precipitation) are showing particularly pronounced response under a certain scenario of global climate change. Characterization of such climate response-based hotspots can provide key information to identify and investigate primary processes of regional-scale climate change (Giorgi, 2006).

Similar to Diffenbaugh and Giorgi, (2012), here we also use the concept of Standard Euclidean Distance (SED) to quantify a new index, named Precipitation based Hotspot Index (PHI) which encapsulates the total change in multi-dimensional precipitation characteristics between the baseline and future periods. This new index considers some additional precipitation change indicators ( $\Delta$ ), compared to some other similar indices used in earlier studies such as Diffenbaugh and Giorgi, (2012) and Turco et al. (2015), and thus presents a more inclusive scenario of changing characteristics of precipitation comprising the changes in the mean and variability of seasonal precipitation, along with the extremes, their magnitude, frequency, and intensity. Mathematically, it is expressed as,

$$PHI = \sqrt{\sum_{i=1}^{N_{\Delta}} \sum_{j=1}^{N_s} \left( \frac{\Delta_{ij}}{\max(|\Delta_{ij}|)} \right)^2} \quad (1)$$

where,  $\Delta_{ij}$  is the  $i^{\text{th}}$  change indicator in the  $j^{\text{th}}$  season at each grid point. Here, we consider total 7 precipitation change indicators (thus,  $N_{\Delta} = 7$ ) for 4 seasons separately: summer, monsoon, post-monsoon and winter (so,  $N_s = 4$ ). These 7 indicators include (i) percentage change in mean precipitation ( $\Delta P$ ), (ii) percentage change in the inter-annual coefficient of variation of the detrended precipitation ( $\Delta P_{\text{var}}$ ), (iii) percentage change in the 95th percentile precipitation ( $\Delta P_{\text{ex}}$ ), (iv) frequency of wetter seasons, i.e., seasons with higher than the maximum precipitation in the base period ( $f_{\text{wet}}$ ), (v) percentage increase in average precipitation in the wetter seasons w.r.t the maximum in the base period ( $\Delta P_{\text{fwet}}$ ), (vi) frequency of drier seasons, i.e., seasons with lower than the minimum precipitation in the base period ( $f_{\text{dry}}$ ), (vii) percentage decrease in average precipitation in the drier seasons w.r.t the minimum precipitation in the base period ( $\Delta P_{\text{fdry}}$ ).

Additional inclusion of three indicators, viz,  $\Delta P_{\text{ex}}$ ,  $\Delta P_{\text{fwet}}$ , and  $\Delta P_{\text{fdry}}$  makes the index PHI more informative than some similar indices as stated earlier. For instance,  $\Delta P_{\text{ex}}$  considers the changes in the level of extreme precipitation. On the other hand,  $f_{\text{wet}}$  and  $f_{\text{dry}}$  take care of the number of seasons with higher than maximum and lower than minimum precipitation in the future and thus consider the frequency information. However, the intensity perspective remains absent, i.e., by what extent this maximum or minimum will shoot above or fall below, respectively, in the future. Hence, the present study includes  $\Delta P_{\text{fwet}}$  ( $\Delta P_{\text{fdry}}$ ), which indicates the percentage change in the average precipitation in the future exceeding (subceeding) the maximum (minimum) precipitation in the base period. Thus, the inclusion of these three additional indicators takes care of the magnitude, frequency, as well as intensity aspect of extreme precipitation. For further clarification about all 7 indicators, readers can see the section A2 of [supplementary information](#), where one hypothetical example is illustrated.

Overall, these seven change indicators ( $\Delta_{ij}$ ) are designed to incorporate various attributes of precipitation such as, mean, variability, extremes – its frequency and intensity into the PHI. Hence different change indicators will have different ranges of their values. Therefore, the  $\Delta_{ij}$  values need to be scaled before summing up to determine PHI, as depicted in eqn. (1). This scaling is done by dividing each change indicator by their maximum absolute value ( $\max |\Delta_{ij}|$ ) across the study area. As our analysis considers two future scenarios (SSP245 and SSP585) and two time periods (Near-future and Far-future), we rescaled each indicator of both the scenarios and time periods using the

maximum value in the far-future period under the highest forcing (i.e., SSP585) across the study area. Thus, this approach yields a relative metric of aggregated precipitation changes that can be directly compared between any regions within the study area, forcing pathways, and future time periods. Overall considering 7 precipitation change indicators for 4 different seasons gives a total of 28 dimensions at each grid point, thus by limiting the values of PHI between zero and  $\sqrt{28} = 5.29$ . However, it must be noted that similar to other earlier indices, the PHI is also a comparative index, which means a small PHI value does not necessarily imply a small absolute change, but only a small climate response compared to other places within the study area. Moreover, from eq. (1) it is evident that this PHI index is bi-directional in nature, i.e., the index cannot differentiate between a place with a strong increase in precipitation and a place with a strong decrease in precipitation, and, designate them as equally problematic under climate change.

### 3.4. Identification of key-vulnerable cities

In order to identify the key-vulnerable cities, we have considered all tier-I cities (total 493 cities within our study area) i.e., the cities with more than 1 lakh population as per census, 2011 in India (<https://www.census2011.co.in/city.php> accessed on August 2021). Vulnerability is an important issue in climate change adaptation and mitigation studies. As per Flato et al., 2013, vulnerability is defined as the propensity of a region to be adversely affected by climate hazards. In other words, vulnerability is the degree to which a system is susceptible to and unable to cope with, the adverse effects of climate change (Parry et al., 2007). Thus, vulnerability becomes a function of (i) climatic exposure or hotspots, and (ii) the coping capacity or adaptability of the region. The coping capacity or adaptability of a region depends on various socio-economic factors such as population density, per-capita income, educational facilities, health infrastructure, technological advancement, economic development, etc. However, the availability and reliability of such socio-economic data are highly questionable. Hence, based on some earlier studies (Ionescu et al., 2009; Torres et al., 2012), we considered two internationally accepted Vulnerability Factors (VFs) with reliable data sources– (i) Population Density (PD) and (ii) inverse of Human Development Index (HDI).

Socio-economic vulnerability is higher for densely populated regions for various obvious reasons such as higher sewage demand, more traffic, more impervious area, etc. On the other hand, socio-economic vulnerability is higher for the regions with lower HDI value. HDI is one of the key global indicators for development, which conveniently combines three important social indicators – health, income, and education, into a single non-dimensional measure between 0 and 1. Low HDI implies a generally low standard of living, such as a poor sanitation system, inadequate health infrastructure, slow economic growth, and low literacy levels. All these factors significantly influence the population's adaptive capacity for climate change, particularly for extreme precipitation. Hence, the inverse of HDI is used as one VF in this study. Therefore, using these two VFs (PD and HDI) along with PHI, we define another index, named Precipitation-based Vulnerability Index (PVI) to identify the key-vulnerable cities across India. PVI can be formulated as,

$$PVI = sPHI \times \sqrt[3]{\prod_{i=1}^N sVF_i} \quad (2)$$

where, PVI is the multiplication of standardised PHI (sPHI) and the geometric mean of the standardised Vulnerability Factors (sVF).  $N (=2)$  is the number of VFs, including PD and inverse HDI. Thus, eq. (2) gets modified as,

$$PVI = sPHI \times \sqrt[3]{sPD \times \frac{1}{sHDI}} \quad (3)$$

where, sPD is the standardised population density and sHDI is the standardised human development index. As the theoretical ranges of

PHI (0–5.29), PD (0–∞) and HDI (0–1) are completely different from each other, they need to be standardised to the same scale before using in eq. (3), which is done by some empirical cumulative distribution function (ecdf). Therefore, the values of PVI get limited between 0 and 1.

To determine future PVI values, the PHI values can be obtained from the future-simulated GCM output, as explained earlier in section 3.3. However, to get future-projected values of PD are obtained from a recent publication by Jones and O’Neill (2016). They developed a new set of global, spatially explicit future population scenarios that are consistent with the new SSPs, and made publicly available (data source: <https://www.cgd.ucar.edu/iam/modeling/spatial-population-scenarios.html>, accessed in August 2022). However, in case of HDI, no such future-projections are available. Hence, here we use the latest available data (for the year 2015) for HDI from Kummur et al. (2018) with a reasonable assumption that its relative spatial distribution will remain more-or-less same over future. This global sub-national scale gridded HDI dataset was prepared based on various Human Development Reports (HDRs) by United Nations Development Programme (UNDP). This data is also publicly available through <https://doi.org/10.5061/dryad.dk1j0> (accessed in August 2022).

### 4. Results and Discussion

#### 4.1. Efficacy of RMPH method for bias correction

Both the RMPH and QM methods of bias-correction are developed between daily-scale IMD observed precipitation data and historically simulated precipitation from each of those 14 GCMs over a common time period 1961–2014. As, both the bias-correction methods are applied on the daily-scale data, it would be indeed required to judge the model performance from the statistics of the bias-corrected series at aggregated time scales (such as monthly or annual). Therefore, the efficacy of these two bias-correction techniques in correcting the bias in daily, as well as aggregated time-scale is examined by considering five precipitation- derived statistics, viz., (i) annual precipitation (P), (ii) monthly precipitation (MP), (iii) 95th percentile of wet day (greater than 1 mm/day) precipitation (P95), (iv) annual maximum daily precipitation (AMDP), and (v) monthly variation of precipitation. Needless to mention, the variables P and MP will be used to judge the effectiveness of bias-correction in aggregated time-scale, P95 and AMDP will be

for two different levels of extremes, and monthly variation will help to confirm the correctness of the seasonal pattern. Further to judge their performance in capturing the low-frequency variability, we considered the standard deviation (SD) of these five statistics, along with their mean.

The results for the first four variables are shown in Fig. 2a for the mean level. It can be observed that the raw simulated GCM output (panel b) mostly underestimates observed precipitation (panel a), especially in case of extremes. On the other hand, the bias-corrected data from both techniques (panels c and d) shows a reasonably improved agreement with the observed data. In particular, the RMPH method shows superiority over the QM method – both in terms of mean and specifically extremes, thus resulting in near-zero value of residual bias (panel g) all over India. This can be further confirmed by Table 2, which shows the quantitative outcome of this comparative analysis between QM and RMPH methods in terms of the all-India averaged value of the multi-model mean bias in both mean, as well as SD. From this table, we can see that although the QM method is successful in reducing the existing bias in raw GCM simulations, the performance of the RMPH method is even better, particularly in case of extremes, both at mean and SD levels. Thus the effectiveness of RMPH method of bias-correction in

**Table 2**  
Comparison of QM and RMPH method of bias correction.

Precipitation Attributes	Statistics	All India averaged Bias in multi-model ensemble mean		
		Raw GCM data	Bias corrected data using QM	Bias corrected data using RMPH
Annual precipitation (mm)	Mean	175.56	47.97	45.15
	SD	148.62	20.94	3.55
Monthly precipitation (mm)	Mean	14.91	3.76	3.99
	SD	34.08	16.00	15.06
95th percentile precipitation (mm)	Mean	23.09	4.22	0.93
	SD	9.30	2.65	0.54
Annual max daily precipitation (mm)	Mean	42.65	28.51	0.51
	SD	23.82	16.37	1.14

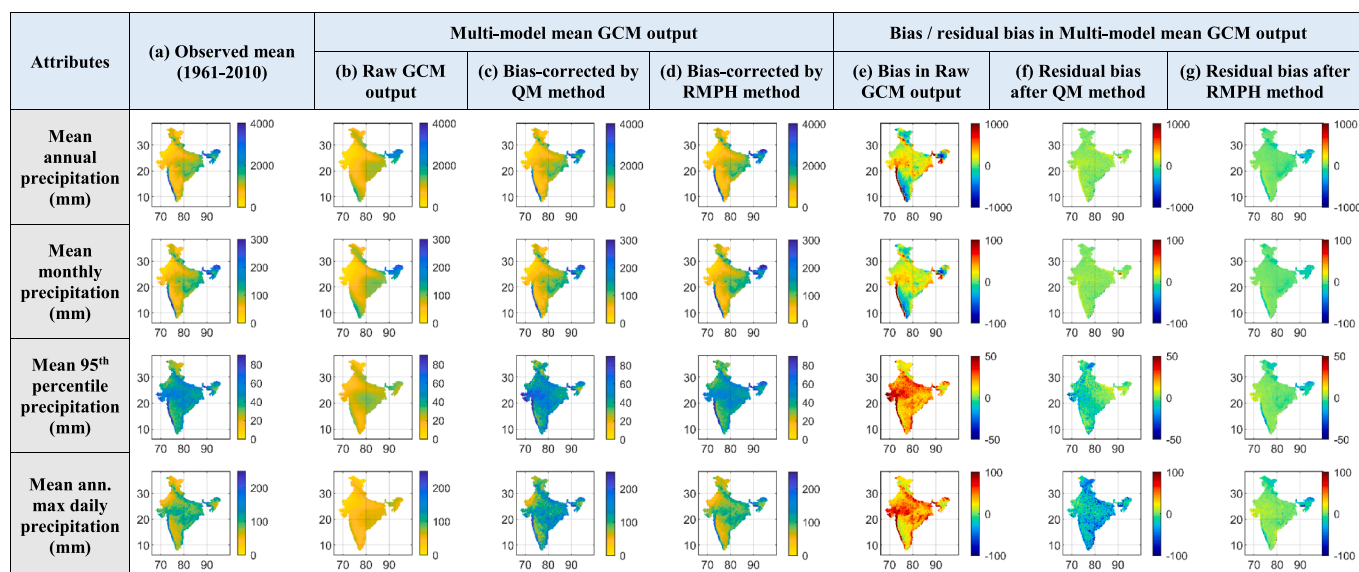


**Fig. 2a.** Results of QM and RMPH method of bias correction, (a) observed mean over 1961–2010, (b) Multi-model mean of raw GCM output, (c, d) Multi-model mean of bias-corrected GCM output using QM and RMPH method, (e) Existing bias in the multi-model raw GCM, and (f, g) residual bias in the bias-corrected GCM output after using QM and RMPH method.

debiasing mean, variability, as well as extremes is established. Similarly, Fig. 2b depicts a better conformity between the observed and bias-corrected monthly variation of precipitation from RMPH method than QM method, averaged over entire Indian mainland. On the contrary, the performance of multi-model raw GCM output is quite poor in capturing the month-wise variation of precipitation over India, even with a very high uncertainty range. This result further strengthens the efficacy of the RMPH method of bias correction. However, in case of bias in trend, although the RMPH method shows comparatively better performance than the QM method, it cannot capture the overall spatial distribution of trend accurately. From supplementary Table S2, it can be noticed that the observed all-India averaged multi-model mean trend in annual precipitation is 0.36 mm/year, the same from QM method is 1.18 mm/year and from RMPH method is 0.81 mm/year. Though the result from RMPH method is closer to the observations, still there is a good scope of improvement in capturing overall spatial pattern of trend. Overall, the RMPH method is found as an effective bias-correction tool, and hence it is used in the present study to debias the raw GCM simulated future precipitation data from 14 CMIP6-GCMs, and used for subsequent analysis. However, we have kept the multi-model multi-scenario dataset from both the bias-correction techniques in an open-source data repository (<https://figshare.com/s/9d978fcff33e86bbf56b>) and expect it to be helpful for impact assessment studies, hydrologic modelling etc.

#### 4.2. Future-Projected changes in precipitation across India

##### 4.2.1. Changes in seasonal variation of precipitation

In this section, we present the future projections of annual precipitation, as well as for four different seasons (viz., summer, monsoon, postmonsoon, winter) and its spatio-temporal evolution across India from an aggregated analysis of 14 state-of-the-art bias-corrected (RMPH method) CMIP6-GCMs. The summary of this assessment for all seasons, two emission scenarios (SSP 245 and 585) and over two future time periods (near- and far-future period) is provided in Figs. 3, 4 and 5 in terms of spatial distribution of changes and trend, bar plots of multi-model ensemble (MME) mean changes and future-projected time series along with uncertainty, respectively. The quantitative outcome of this analysis (i.e., MME mean and its 95% confidence interval), averaged over entire India (except the north-most hilly region) is provided in Table 3. Similar table for all six HPZs can be found in Table S3 of supplementary information.

Fig. 3 (first row) depicts an overall increase in annual precipitation in all parts of India over future under both the scenarios, except a small portion of northeast India, where some minor reduction is visible in near-future under SSP245. Overall in terms of absolute changes (panel a), the central part of India, Western Ghats, and northeast India show considerable increase, thus resulting in maximum amount of increase in

the high-precipitation zones such as, HPZ-3 and HPZ-6 (see Fig. 4). However, in terms of percentage change (panel b), low precipitation zones (HPZ-1 or HPZ-4) shows the highest amount of increase, causing a substantial increase in northwest and southern part of the country, as confirmed by panel b of Fig. 3. Also, we see the extent of increase (both absolute and percentage) gets stronger with the passage of time (in far-future) and under higher forcing scenario (i.e., SSP585). Annual precipitation is projected to increase by 188.85 mm (147.99 mm) in near future, and by 530.04 mm (288.99 mm) in the far future period under SSP585 (SSP245) scenario, over its average value of 1152 mm in the base period (1981–2010). If we observe the time series plot or probability density functions (pdfs) of annual precipitation (Fig. 5), not much difference is visible between both the scenarios in near-future period, i. e. up-to 2060. However, the far-future period, the difference between SSP245 and SSP585 becomes significantly pronounced; the time series becomes more or less stationary in SSP245 (green line), but keeps on increasing significantly under SSP585 (red line) - probably indicating more anthropogenic activities towards end of this century (EOC). This observation is also reflected in the trend plots of annual precipitation (panel c of Fig. 3), where mostly similar pattern and magnitude of trend can be seen in near-future period under both the scenarios. However, in far-future period, most part of India is not showing any significant trend (at 5% significance level, shown by grey colour in maps) under SSP245, whereas on the contrary, almost entire India is having some statistically significant trend towards EOC under SSP585. In quantitative terms, MME mean trend of 55.20 mm/decade (51.08 mm/decade) in near-future period across India gets strengthened (weakened) in the far-future period with a MME mean trend of 107.77 mm/decade (23.48 mm/decade) following SSP585 (SSP245). Now it will be interesting to investigate how this increase in annual precipitation gets distributed among four different seasons.

Similar to annual precipitation, summer or pre-monsoon precipitation (MAM) also shows an overall increasing pattern across India which gets more intense from near- to far-future period and under SSP585 (second row, Fig. 3). In terms of absolute changes, maximum amount of increase is visible in the eastern and north-eastern part of the country. In contrast, the high-seasonality zones (HPZ-1, 2 and 3) shows the maximum amount of percentage increase in summer precipitation (Fig. 4). The average summer precipitation magnitude of 120.47 mm over the base period is projected to increase by 24.97 mm (12.67 mm) in the near-future and, by 56.69 mm (22.94 mm) in the far-future period following SSP585 (SSP245). Unlike annual precipitation, most part of India does not show statistically significant trend in summer precipitation over future, with a maximum MME mean trend of 9.59 mm/decade across India in the far-future period under the worst emission scenario.

The changing pattern of monsoon precipitation (JJAS) is quite similar (third row, Fig. 3) to that of annual precipitation (because of its

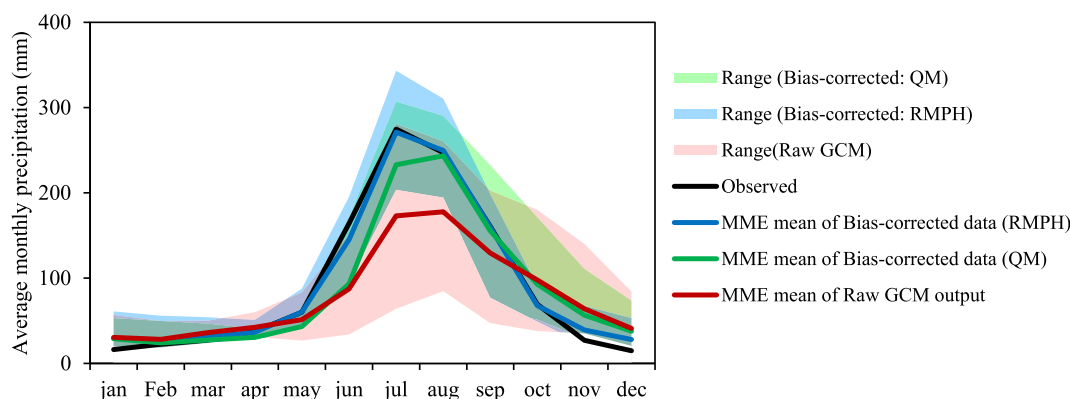


Fig. 2b. All-India monthly variation of precipitation from observed data (black), raw GCM data (red) and bias-corrected GCM data from RMPH (blue) and QM (green) method. The shaded area represents uncertainty (range) of all 14 CMIP6-GCMs. (For interpretation of the references to color in this figure legend, the reader is referred to the web version of this article.)

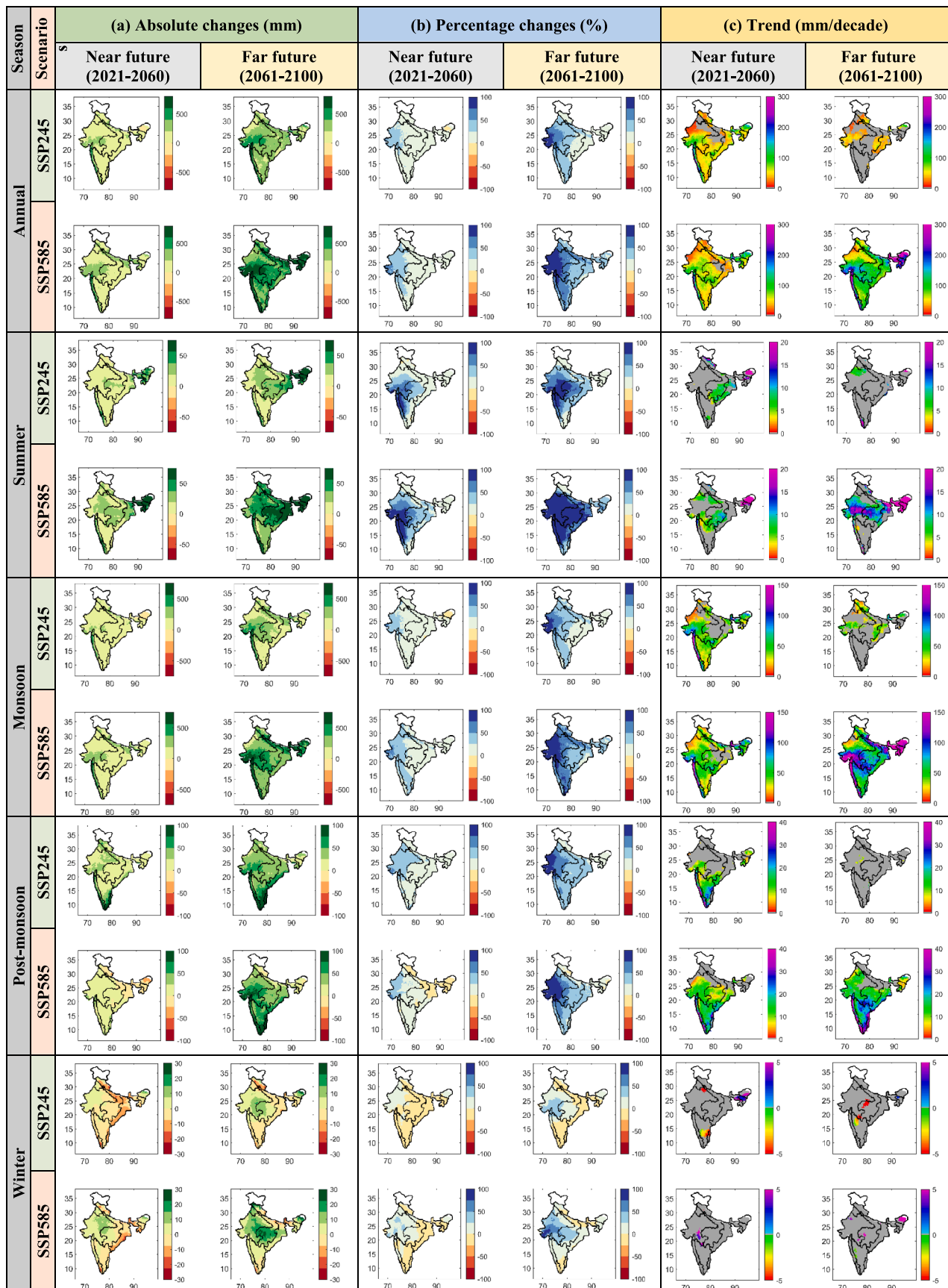
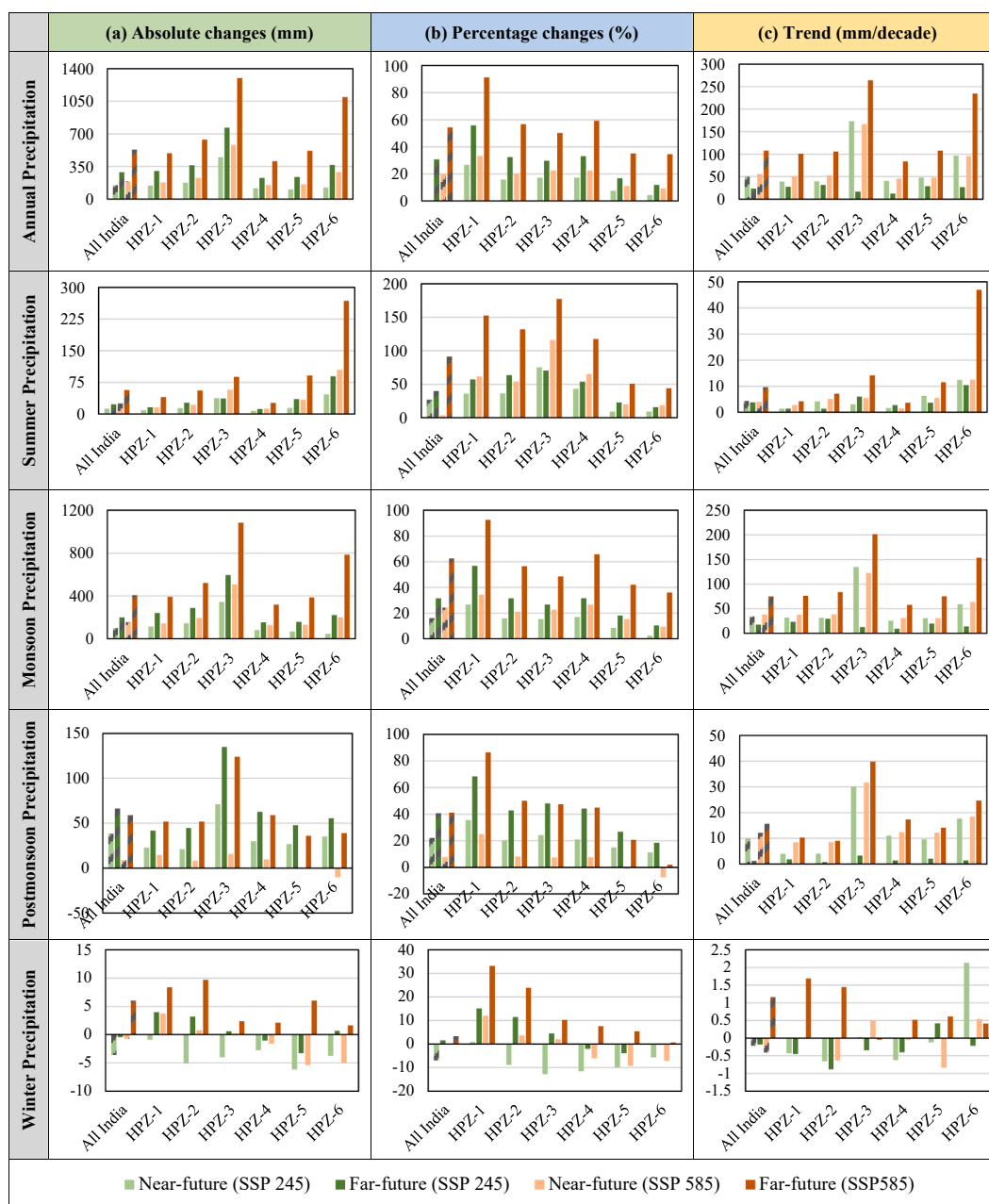


Fig. 3. MME mean changes in seasonal precipitation and trend across India over future.



**Fig. 4.** MME mean of (a) absolute changes, (b) percentage changes, and (c) trend in seasonal precipitation across India over future following two scenarios confidence interval, averaged across India over 1981–2100, and (b) corresponding underlying pdfs over near- and far-future period following two scenarios.

~ 70% contribution in total annual precipitation). Here also, we observe the same portion in northeast India is showing some slight reduction in monsoon precipitation in near-future under SSP245. Likewise, the Western Ghats and central part of India is showing good amount of absolute changes, whereas the low-precipitation zones (HPZ-1 and 4) are having the maximum amount of percentage changes w.r.t the base period (Fig. 4). The average monsoon precipitation of 785.85 mm over the base period is expected to be increased by 408.47 mm (200.04 mm) towards EOC following SSP585 (SSP245). The observations of trend analysis and time series plots are again quite similar to that of annual precipitation, i.e., a more or less similar pattern up to mid-century and then gradual weakening or strengthening of trend following SSP245 and SSP585, respectively.

In case of post-monsoon precipitation (OND), a very interesting observation is made. Unlike earlier cases, higher extent of increase is witnessed under the lower forcing scenario, i.e., SSP245 than SSP585 in

case of post-monsoon precipitation. Even in case of SSP585, some reduction is noticed in eastern part of India, together with northeast India and along the Himalayan foothills (fourth row, Fig. 3). As expected, maximum amount of absolute changes can be seen in the southern part of the country, where the influence of northeast monsoon is most. However, in terms of percentage changes, HPZ-1, i.e. the northwest part of India shows the highest level of increase than other HPZs (fourth row, Fig. 4). Overall 38.52 mm and 66.46 mm increase over the average value of 181.10 mm is projected in near- and far-future period, respectively under SSP245 scenario. Whereas, the same under SSP585 is quite less; only 9.05 mm and 58.55 mm in near- and far-future period, respectively. These observations can further be confirmed from the time series and pdf plots as in Fig. 5 (fourth row), which shows a clear dominance of SSP245 over SSP585, except the last decade of the century. Trend analysis of post-monsoon precipitation reveals maximum trend in the southern part of the country, whereas the northern India

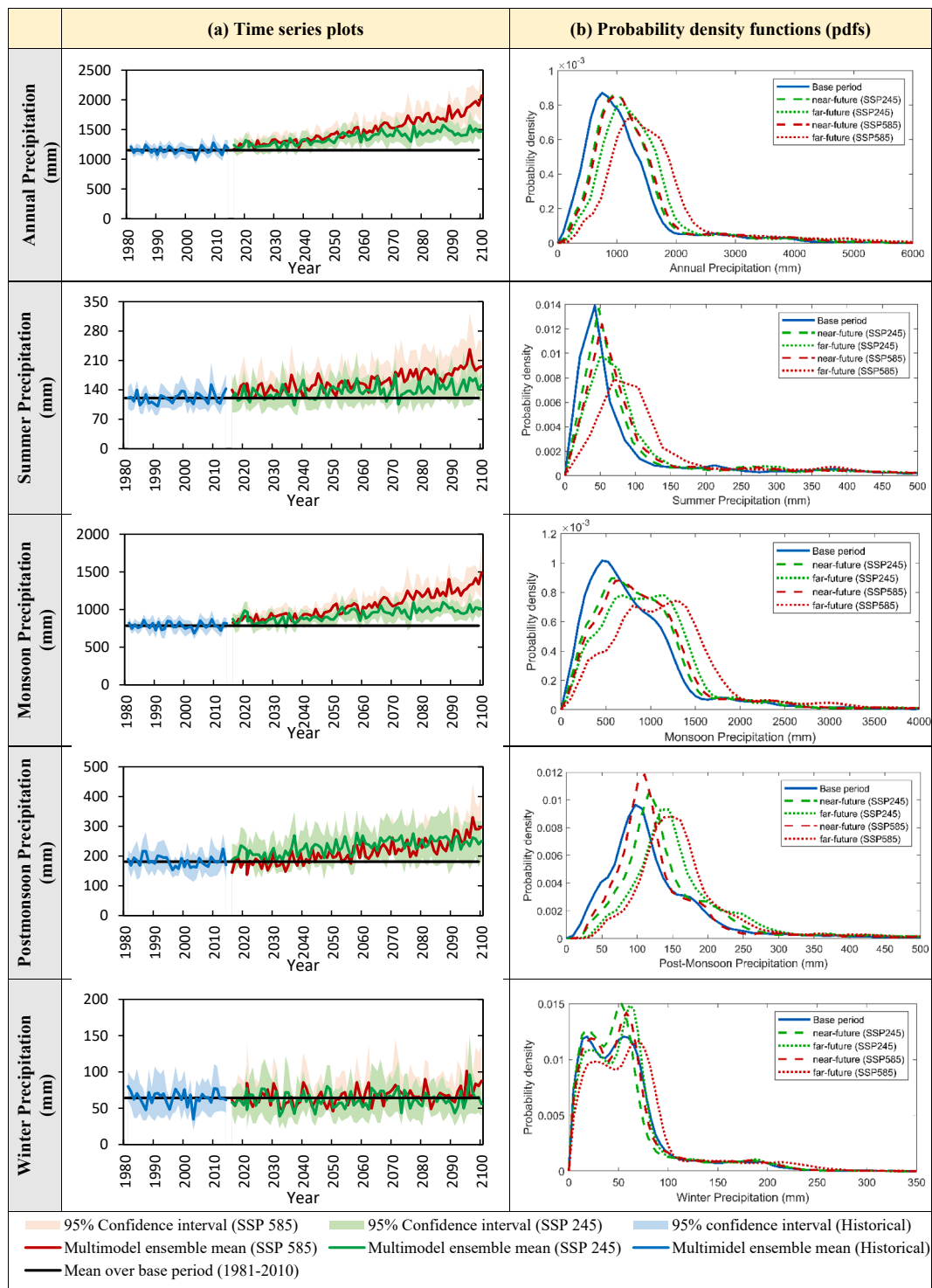


**Fig. 5.** (a) MME mean annual time series plots of seasonal precipitation and its 95% confidence interval, averaged across India over 1981–2100, and (b) corresponding underlying pdfs over near- and far-future period following two scenarios.

mostly remains statistically insignificant. Across India, MME mean trend of 15.66 mm/decade is expected in the far-future period following SSP585 scenario.

In general, India receives very less amount of precipitation (~6% of annual precipitation) in winter season (JF). However, this multi-model analysis projects even lesser amount of winter precipitation in future. From spatial analysis, a decline in winter precipitation is observed in most part of the country, especially in eastern part, southern part and along Himalayan foothills. However, this extent of declination gets

reduced with the passage of time and under higher forcing scenario. Nonetheless, some amount of increase is also visible in the northwest part of the country (HPZ-1), especially in the far-future period. The Fig. 5 (last row) depicts the time series of winter precipitation having no clear trend, remains mostly same as of its base period. Similarly, the underlying pdfs in future periods do not show any shift from that of base period. Overall across India, MME mean reduction of 3.60 mm and 0.45 mm is projected in near- and far- future period following SSP245. On the other hand, under SSP585, MME mean reduction of 0.72 mm is

Table 3

MME mean absolute changes, percentage changes and trend in seasonal precipitation in future, averaged over entire India along with its 95% confidence interval following two different scenarios.

Seasons		Annual precipitation		Summer precipitation		Monsoon precipitation		Postmonsoon precipitation		Winter precipitation	
Mean over base period (mm)		1152		120.47		785.85		181.10		64.17	
scenario	Time period	Absolute Changes (mm) (% Changes)	Trend (mm/dec ade)	Absolute Changes (mm) (% Changes)	Trend (mm/dec ade)	Absolute Changes (mm) (% Changes)	Trend (mm/dec ade)	Absolute Changes (mm) (% Changes)	Trend (mm/dec ade)	Absolute Changes (mm) (% Changes)	Trend (mm/dec ade)
SSP 245	near future	147.99 ± 105.74 (15.8 ± 9.93)	51.08 ± 26.08	12.67 ± 44.53 (26.80 ± 65.77)	4.32 ± 4.13	100.40 ± 125.56 (16.18 ± 18.53)	34.44 ± 18.06	38.52 ± 69.89 (22.15 ± 42.6)	9.96 ± 7.6	-3.60 ± 24.37 (-6.92 ± 49.07)	-0.22 ± 2.25
	far future	288.99 ± 151.67 (30.66 ± 14.64)	23.48 ± 16.11	22.94 ± 49.19 (39.67 ± 71.76)	3.78 ± 4.08	200.04 ± 160.53 (31.47 ± 23.76)	17.82 ± 13.74	66.46 ± 80.99 (40.70 ± 51.05)	1.24 ± 6.63	-0.45 ± 25.87 (1.58 ± 53.94)	-0.18 ± 1.75
SSP 585	near future	188.85 ± 134.95 (19.82 ± 12.84)	55.20 ± 28.69	24.97 ± 49.7 (43.43 ± 75.31)	3.95 ± 3.85	155.54 ± 146.77 (24.29 ± 21.55)	38.14 ± 20.6	9.05 ± 61.25 (7.75 ± 39.36)	12.15 ± 6.96	-0.72 ± 23.9 (-0.01 ± 48.44)	-0.41 ± 2.5
	far future	530.04 ± 260.78 (54.27 ± 25.72)	107.77 ± 30.99	56.69 ± 68.96 (91.1 ± 111.76)	9.59 ± 5.18	408.47 ± 256.43 (62.54 ± 38.1)	75.28 ± 25.34	58.85 ± 75.69 (41.16 ± 51.16)	15.66 ± 7.27	6.03 ± 31.93 (13.27 ± 64.29)	1.16 ± 2.95

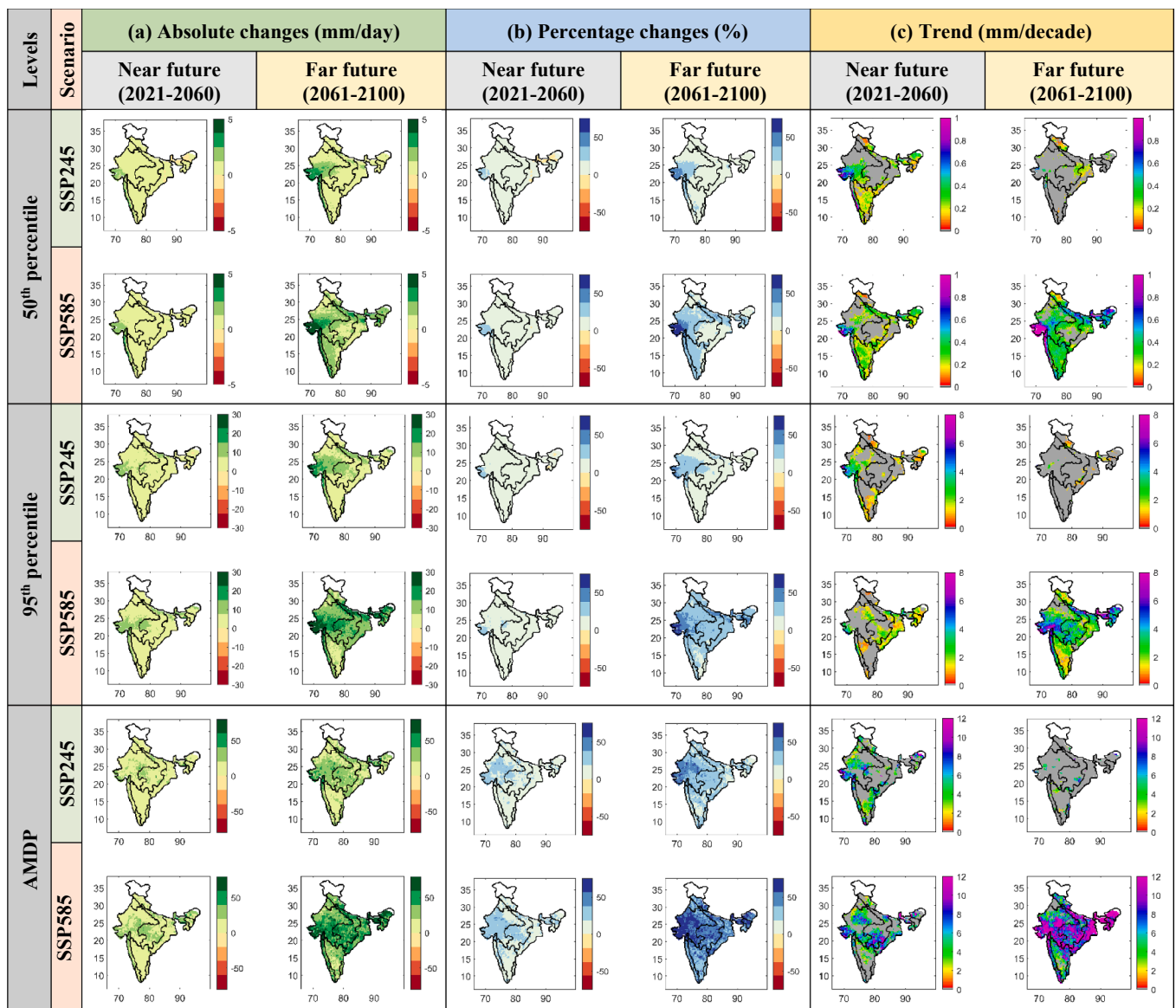


Fig. 6. MME mean changes in different levels of (extreme) precipitation and trend across India over future.

projected in near-future, which will be evolved as 6.03 mm increase in far-future period. Trend analysis also reveals that more than 90% of Indian mainland does not show statistically significant trend in winter precipitation, barring a few scattered places.

Overall this multi-model analysis gives a robust signal of wetter climate for entire India, having the obvious spatial diversity and inter-model uncertainty, with major contribution coming from summer and monsoon season, and relatively weaker or negative contribution from post-monsoon and winter precipitation. Generally, the low-precipitation zones, especially HPZ-1 is showing consistent increase in precipitation in all seasons. Further, the level of increase in precipitation across all HPZs are getting enhanced with time and under the highest forcing, indicating the possible impacts of anthropogenic activities towards changing pattern of climate.

4.2.2. Changes in different levels of (extreme) precipitation

In this section, we present the multi-model projected changes in different levels of extreme precipitation in future across India. Towards this, we have considered two different levels of measures for extreme precipitation- (a) 95th percentile of wet-day precipitation (P95), and (b) annual maximum daily precipitation (AMDP). Additionally, to compare the changes in the level of extremes with that in the level of mean, we have also considered the median or 50th percentile of wet-day precipitation (P50). The analysis is exactly same as in case of seasonal precipitation, i.e., the absolute changes, percentage changes in different levels of precipitation are evaluated, along with a trend analysis under two forcing pathways. The results are summarized in Figs. 6, 7 and 8 in terms of spatial distribution, bar plots, and time series plots with uncertainty in projection, respectively. Furthermore, the quantitative outcomes of this analysis are presented in Table 4 in terms of MME mean changes along with its uncertainty band (95% confidence interval).

In general, a similar pattern of increase is noticed in case of 50th and 95th percentile precipitation in terms of the spatial distribution (Fig. 6).

The increase is mostly observed in the Westerns Ghats, Gujrat portion, and north-central part of India. Largely the high-seasonality zones such as, HPZ-1, 2 and 3 are projected to have the maximum amount of increase (Fig. 7). Similar to seasonal precipitation, here also, the amount of increase gets more intensified towards EOC and under the worst scenario (SSP585). However the extent of percentage increase is higher in case of 95th percentile than 50th percentile. For instance, 22.66% (12.84%) MME mean increase is projected for 50th percentile in the far-future period, whereas the same for 95th percentile is 25.66% (13.74%) following SSP585 (SSP245). The difference becomes even more pronounced in case of the higher level extreme, i.e., AMDP, which is reported to be increased by 44.85% (24.87%) w.r.t the base period towards EOC following SSP585 (SSP245) - almost double increase than the increase in median precipitation. This indicates that, though both mean and extreme precipitation are increasing under the changing climate, the rate of increase is much higher in case of extremes than mean, which is expected to have more detrimental impacts on society including flooding, crop damages, health hazards, erosion, and water contamination problems (Guhathakurta et al., 2011; Pall et al., 2011; Rajeevan et al., 2008).

From the trend analysis (panel c, Fig. 6), we see that most southern India and some part of western India is having statistically significant trend in future, whereas northern India mostly remains statistically insignificant except in far-future period under SSP585. Generally the high-seasonality zones are showing maximum amount of trends, although the HPZ-6 is also showing good amount of trend in AMDP towards EOC. Averaging the trends over entire India, MME mean value of 0.35, 2.33 and 7.07 mm/decade is reported for P50, P95 and AMDP, respectively in the far-future period under SSP585.

The key observations from time series plots and underlying pdfs (Fig. 8) of all three levels of precipitation for future time periods remain mostly same as that in seasonal precipitation. A continuous temporal evaluation towards wetter side is observed in all three levels following

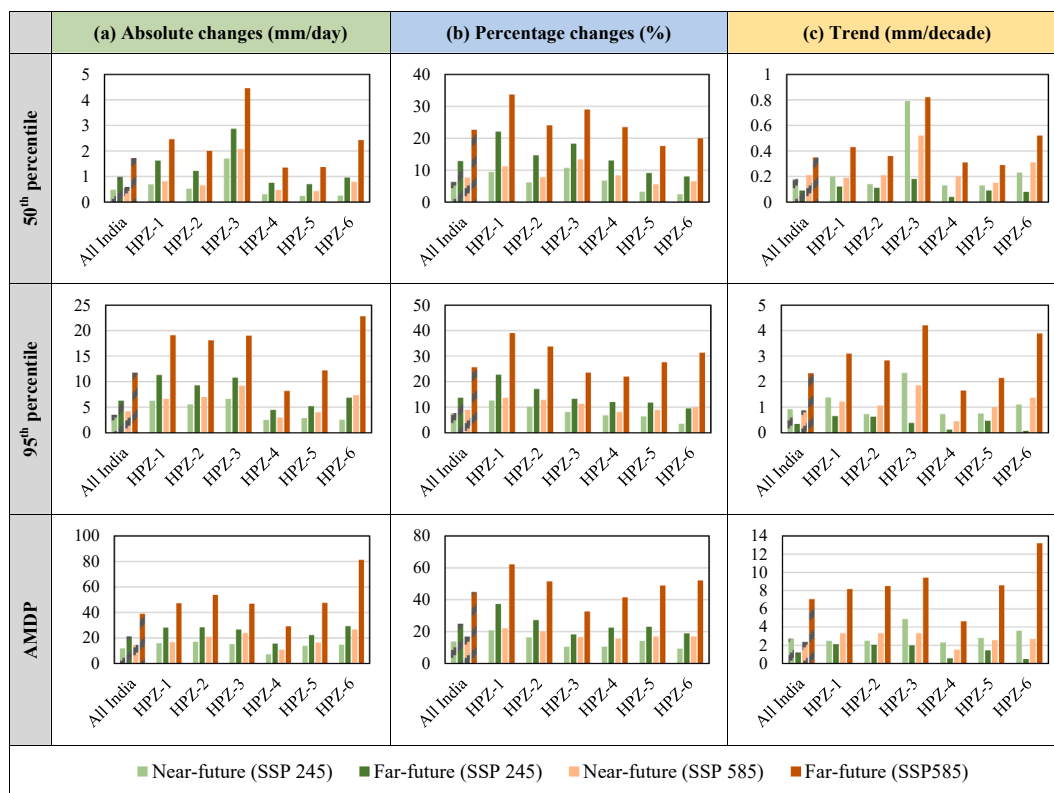


Fig. 7. MME mean of (a) absolute changes, (b) percentage changes, and (c) trend in various levels of (extremes) precipitation across India over future following two scenarios.

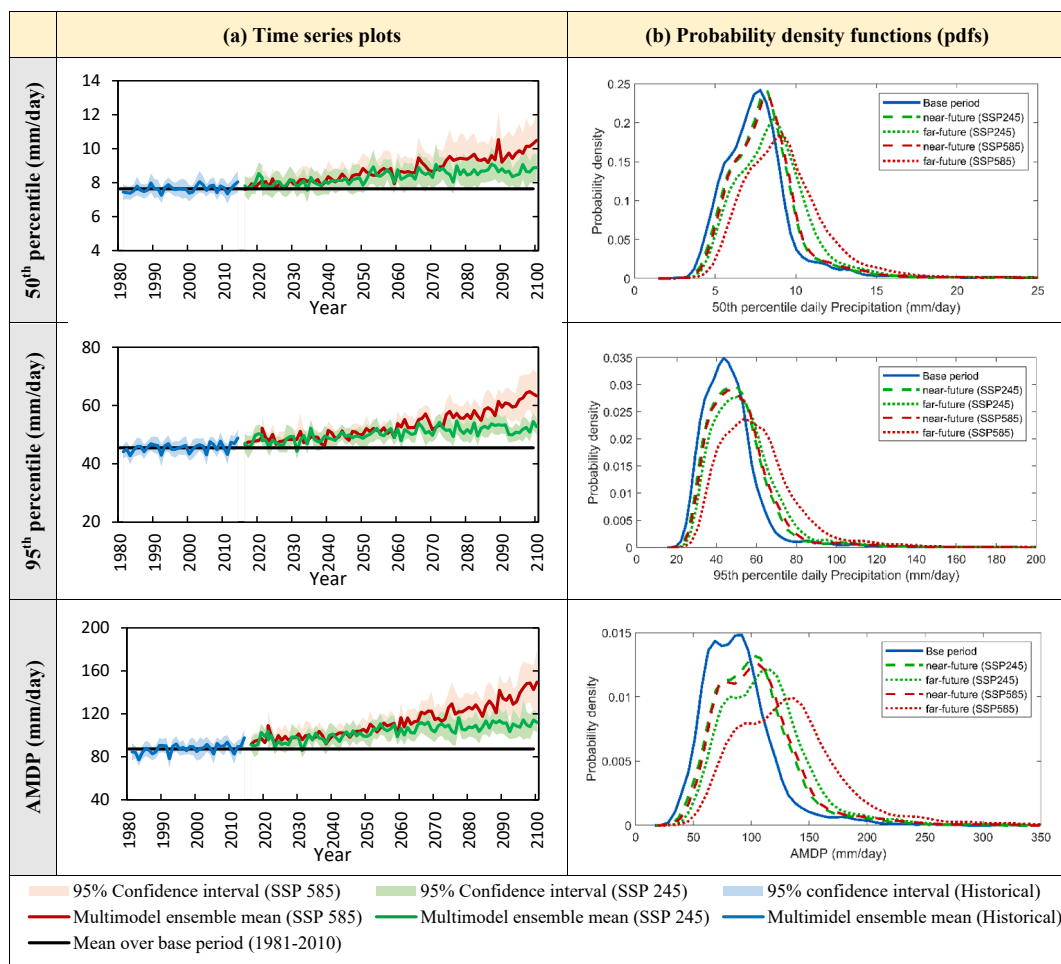


Fig. 8. (a) MME mean annual time series plots of different levels of (extremes) precipitation and its 95% confidence interval, averaged across India over 1981–2100, and (b) corresponding underlying pdfs over near- and far-future period following two scenarios.

Table 4

MME mean absolute changes, percentage changes and trend in different levels (extremes) of precipitation in future, averaged over entire India along with its 95% confidence interval following two different scenarios.

Different levels		50 <sup>th</sup> percentile		95 <sup>th</sup> percentile		AMDP	
Mean over base period (mm/day)		7.64		45.46		87.32	
scenario	Time period	Absolute Changes (mm) (% Changes)	Trend (mm/dec ade)	Absolute Changes (mm) (% Changes)	Trend (mm/dec ade)	Absolute Changes (mm) (% Changes)	Trend (mm/dec ade)
SSP 245	near future	0.48 ± 0.76 (6.28 ± 9.34)	0.18 ± 0.09	3.54 ± 3.37 (7.72 ± 7.29)	0.92 ± 0.53	11.86 ± 8.16 (13.78 ± 9.48)	2.72 ± 1.41
	far future	0.98 ± 0.96 (12.84 ± 11.76)	0.09 ± 0.08	6.30 ± 4.11 (13.74 ± 8.89)	0.34 ± 0.37	21.21 ± 10.67 (24.87 ± 12.49)	1.21 ± 1.13
SSP 585	near future	0.59 ± 0.86 (7.70 ± 10.57)	0.21 ± 0.15	4.21 ± 3.67 (8.97 ± 7.99)	0.88 ± 0.55	14.64 ± 9.72 (16.85 ± 11.3)	2.37 ± 1.36
	far future	1.72 ± 1.52 (22.66 ± 19.02)	0.35 ± 0.17	11.89 ± 6.71 (25.66 ± 14.63)	2.33 ± 0.86	39.06 ± 17.93 (44.85 ± 20.58)	7.07 ± 3.16

both the emission pathways. However till the year 2060, i.e., in the near-future period, not much difference is observed between SSP245 and SSP585. However, after 2060, the time series of all three levels of precipitation mostly remains stationary under SSP245 (green line), whereas

the plots for SSP585 (red line) keep on increasing, thus resulting in almost two-times more increment towards EOC than SSP245. Furthermore, the time series plots depict more pronounced increase above the baseline in case of extremes (especially AMDP) than median

precipitation. Similar observations can also be confirmed from the pdfs (panel b, Fig. 8). The pdfs in near-future period under SSP245 and SSP585 does not have much difference, however in the far-future period, considerable shift towards higher values is observed. Moreover the general nature of shift in pdfs in future periods is more noticeable in case of extremes than that in median precipitation.

4.2.3. Changes in monthly variation of precipitation

Fig. 9 shows the MME mean monthly cycle of precipitation over future periods across India and its six HPZs following two scenarios. A common observation from all the plots is an unequivocal increase in monthly precipitation, especially for the high-rainfall months. However the dry months (Dec to March) mostly remain dry or gets even drier. Noticeable amount of increase starts since summer months like April and May, and reaches maximum in late monsoon months like August and September. In general, the seasonal pattern does not get disturbed, rather get intensified across all six HPZs over future. Similar to our earlier findings, here also maximum amount of increase is visible in case of low-precipitation zones such as, HPZ-1 and 4, and least increase in high-precipitation zones (HPZ-3 and 6).

4.3. Precipitation-based climate changes hotspots across India over future

As explained in section 3.3, seven precipitation change indicators are evaluated and rescaled for all four seasons for each 14 CMIP6-GCMs, followed by calculation of their MME mean and finally the PHI over future periods following two forcing pathways. The final result is shown in Fig. 10 in the form of spatial distribution of PHI or in other words, precipitation change susceptibility maps over near- and far-future period, under SSP245 and SSP585. The places with high (low) values of PHI indicates high (low) susceptibility to precipitation changes. Thus the dominant changing pattern with high values of PHI emerges in northwest, western coast and northeast part of the country towards EOC

under both scenarios. Western states like Gujrat, Maharashtra, Rajasthan, and north-eastern states like Assam show the maximum values of PHI indicating significant level of precipitation changes in future. On the other hand, northern states such as, Punjab, Haryana, Uttarakhand, Uttar Pradesh- mostly in the Gangetic plain, Gangetic west Bengal, or eastern coastal regions of Andhra Pradesh shows comparatively lower values of PHI, depicting lesser degree of changes in precipitation. However, all these less susceptible places also exhibit increase in PHI, i. e., increasing susceptibility with the passage of time in future.

Interestingly, in the near-future period, some parts of coastal Odisha shows distinctly high values of PHI than other obvious aforementioned places like northwest or western coastal regions of India. This can be explained with the help of supplementary Fig S2 or S4, which shows the actual and rescaled values of all 7 indicators for all 4 seasons in near-future period following SSP245 and SSP585. From these figures, we observe that, the variability of precipitation especially in post-monsoon season has particularly increased in that region. Along with that, the number of drier seasons has significantly increased over most of the seasons, with reduction in winter and post-monsoon precipitation in that portion in near-future. Though this indicates drying in true sense, and the PHI being bidirectional in nature, gives a very high value compared to other places in India. However in the far-future period, various places in northwest India, western coast, southern part, and northeast India emerges as highly susceptible hotspot regions because of high values of various indicators such as,  $\Delta P$ ,  $\Delta P_{var}$ ,  $\Delta P_{ex}$ ,  $f_{wet}$ ,  $\Delta P_{f_{wet}}$  (See supplementary Fig. S3 and S5) - all indicating wetter future over those regions. In general, increase in PHI values is observed across the country with the passage of time and under the worst emission scenario SSP585-very similar to our earlier observations on changes in seasonal or extreme precipitation.

Therefore, considering the PHI map over far-future period and SSP585, the precipitation based climate changes hotspots are identified over India. At first, a non-parametric Kernel pdf of PHI is developed for

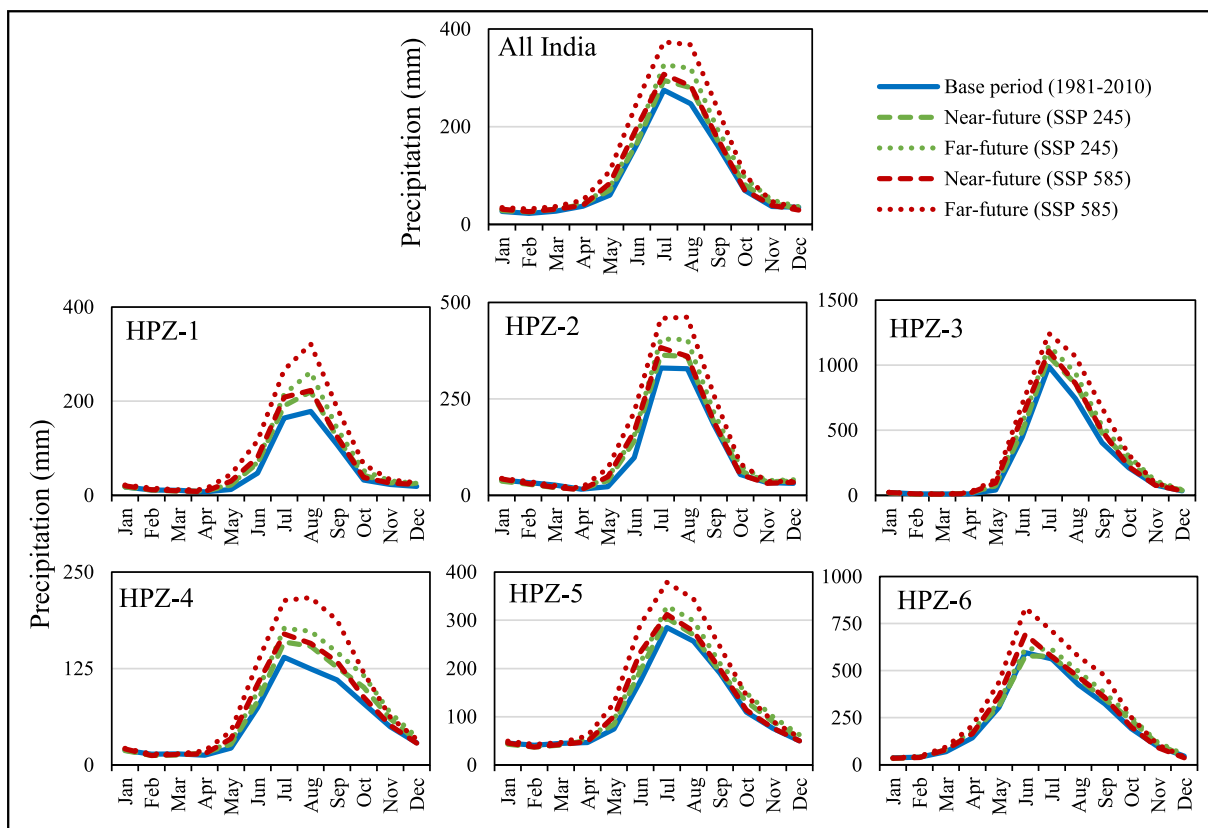


Fig. 9. MME mean changes in monthly variation of precipitation, averaged across entire India and its six HPZs over future following two scenarios.

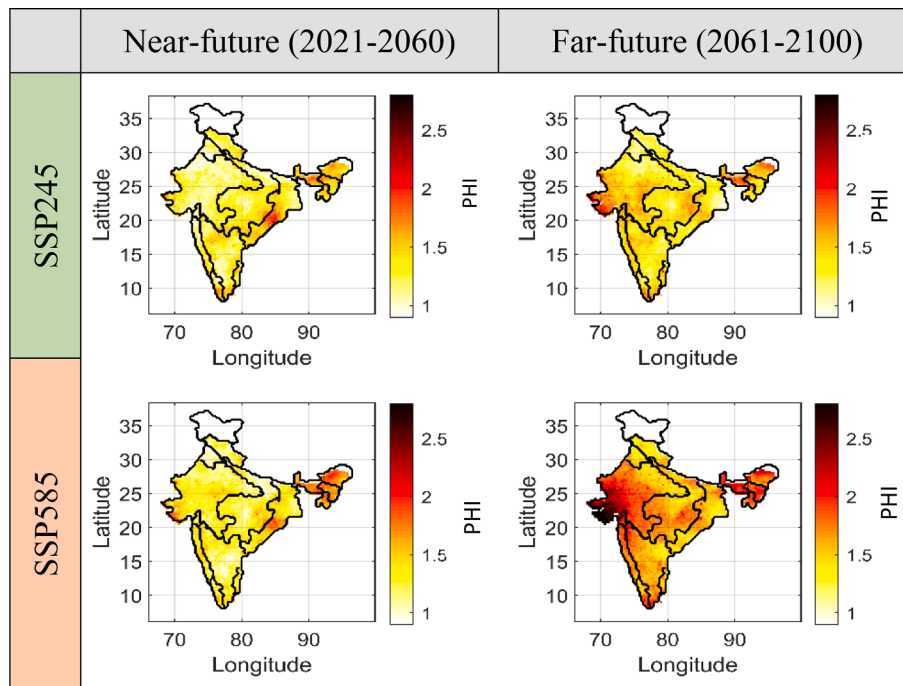


Fig. 10. Temporal evolution of precipitation-based climate changes hotspots across India over future following two scenarios.

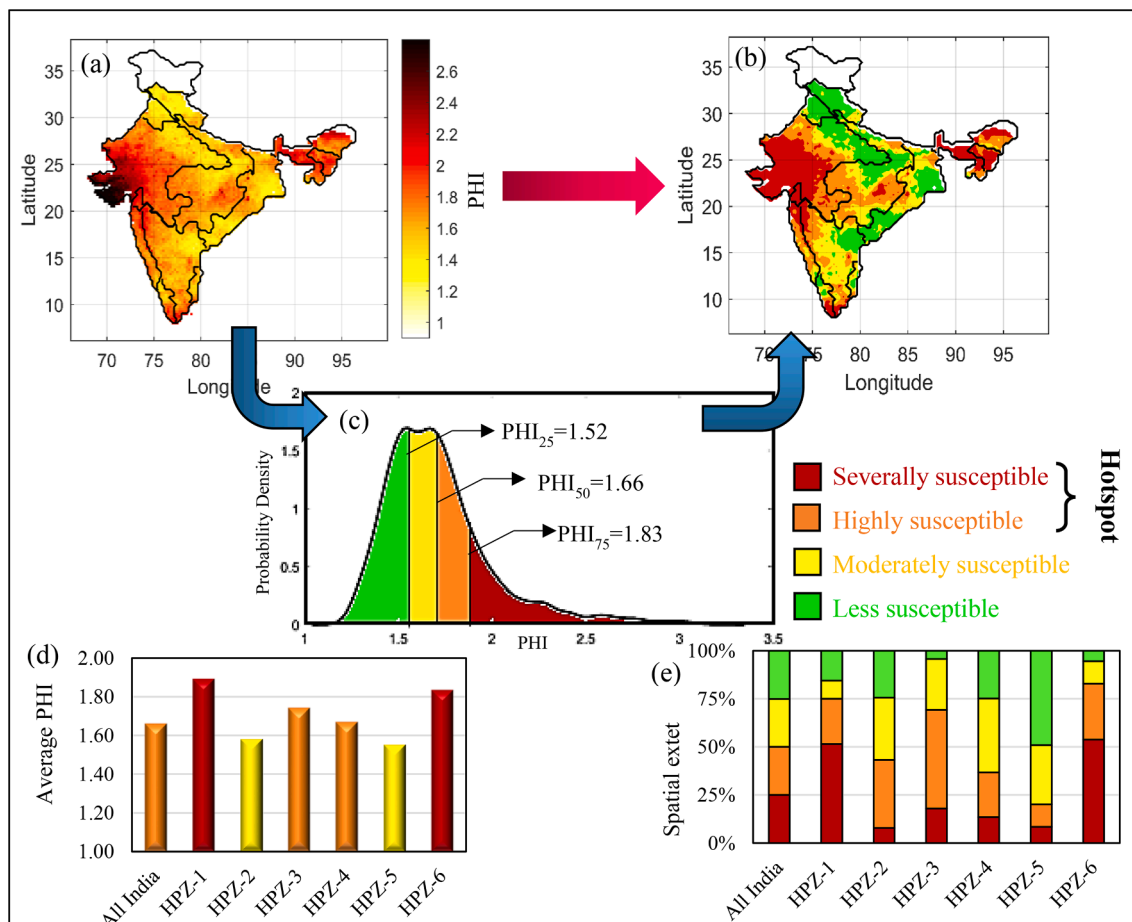


Fig. 11. Development of precipitation changes hotspot map for India in far-future under SSP585. (a) Actual spatial distribution of PHI in far-future under SSP585, (b) Transformed hotspot map having 4 zones, using (c) the pdf of PHI across India. (c) Average values of PHI across HPZs and (d) % of spatial extent under all four colour zones across HPZs.

all grid-points across India for the aforementioned time period and scenario. Then the area under the pdf is split into four different parts on the basis of 25th, 50th, and 75th percentile of PHI values, and accordingly the entire India mainland is categorised into four susceptibility zones- (i) Severely susceptible zone (Red zone):  $\text{PHI} > \text{PHI}_{75}$ , (ii) Highly susceptible zone (orange zone):  $\text{PHI}_{50} < \text{PHI} < \text{PHI}_{75}$ , (iii) Moderately susceptible zone (yellow zone):  $\text{PHI}_{25} < \text{PHI} < \text{PHI}_{50}$ , and (iv) Less susceptible zone (green zone):  $\text{PHI} < \text{PHI}_{25}$ . Out of these four zones, the first two (red and orange zones) are recognised as “precipitation-based climate changes hotspots” in this study. The finally obtained zoned hotspot map is shown in Fig. 11b. Further analysis on spatial distribution of these hotspots across HPZs reveals that the HPZ-1 and HPZ-6 have the maximum spatial extent of hotspots. More than 75% area in these two zones are susceptible to high to severe changes in precipitation over future (Fig. 11d). Moreover, the area-averaged values of PHI over both these two zones are higher than  $\text{PHI}_{75}$  (~1.83) - hence marked as red bar in Fig. 11d. Interestingly, the fundamental reason for both these zones of completely different nature of precipitation characteristics (HPZ-1: Low precipitation-high seasonality; HPZ-6: High precipitation-low seasonality), to be recognised as hotspots is different. The high value of PHI over HPZ-1 is attributed from very high level of increase in mean and extreme precipitation, but variability of precipitation has hardly changed (rather some reduction is noticed) over all four seasons in that zone (supplementary Fig. S5). On the contrary, the HPZ-6 shows lesser extent of increase in  $\Delta P$  or  $\Delta P_{\text{ex}}$ , but the precipitation variability has increased substantially in this zone, with consequently increasing values of  $f_{\text{wet}}$  and  $f_{\text{dry}}$  for various seasons (supplementary Fig. S5). Thus, both these zones of drastically distinct precipitation climatology gets simultaneously identified as hotspots, but for different reasons. Apart from these two zones, the HPZ-3 i.e., the Western Ghats region also shows high value of area-averaged PHI (~1.74) with approximately 70% area exposed to high to severe changes in precipitation. However, unlike HPZ-1 and 6, here major contribution towards this 70% area of hotspot comes from orange zone, not from red zone. Thus the average PHI value (~1.74 <  $\text{PHI}_{75}$ ) is also quite lesser than HPZ-1 or 6, hence marked as orange in Fig. 11d. On the other hand, in cases of HPZ-2, -4 and -5, less than 50% of their area is exposed to hotspots. For HPZ-5, the spatial extent is least- only 20%, thus in turn resulting in the minimum value of area-averaged PHI (~1.55; yellow bar in Fig. 11d) as well. Overall, approximately, 50% of Indian mainland is expected to be precipitation-based climate changes hotspots towards EOC.

Additionally, we developed the hotspot map for India over the recent past (1981–2020), with reference to 1951–1980 period using the IMD-gridded observations (supplementary Fig. S6). A reasonably good similarity can be noticed between the observed and future-projected hotspot maps (e.g., the north-east portion, Western Ghats, southern India, parts of north-west India) along with some expected mismatches as well (e.g., parts of eastern coast, northern and western India). It is now well-established fact that, Earth’s climate has changed in past (Sarkar and Maity, 2021; Trenberth et al., 2003), and will continue to change in future too (Madakumbura et al., 2019). However, the spatio-temporal pattern of changes might not remain same over the time. Thus, such alteration in the hotspot pattern between the observed or historical and future hotspot is expected, and does not contradict our findings.

#### 4.4. Key-vulnerable cities for precipitation change across India over future

Similar to the hotspot maps, we further develop the future precipitation-based vulnerability map for India using the proposed index PVI for near- and far-future periods, following both SSP245 and SSP585 scenario. To develop these maps, the earlier obtained PHI values are used, along with future-projected PD data (for the year 2060 and 2100) and latest-available HDI data (year 2015). The final result is shown in supplementary Fig. S7, which shows the spatial distribution of PVI or in other words, precipitation-based vulnerability maps. Similar to hotspot map, the entire Indian mainland is categorised into four different zones

of vulnerability (supplementary Fig. S8) on the basis of the PVI values in far-future period following SSP585. A compare between the final hotspot map (Fig. 11b) and the vulnerability map (supplementary Fig. S8b) reveals an interesting observation. Although the parts of western India including the Thar desert, Rann of Kutch, parts of northeast India, parts of Kerala are identified as hotspots with high climatic exposure, these are not highly vulnerable because of very less PD or high HDI (for Kerala). On the contrary, in spite of having low to moderate climatic exposure, Himalayan foothills including parts of Uttar Pradesh, Bihar and North Bengal, parts of Odisha and Chhattisgarh are identified as highly vulnerable regions, because of very high PD or low HDI over those places.

Finally, on the basis of the vulnerability map in far-future period following SSP585, we identify the key-vulnerable cities with changing precipitation characteristics. Towards this, we have considered all tier-I cities (total 493 cities within our study area) i.e., the cities with more than 1 lakh population as per census, 2011 in India (<https://www.census2011.co.in/city.php> accessed on August 2021). Out of those 493 cities, 202 cities, i.e., 41% cities are identified as vulnerable cities (red + orange zone) with expected high to severe changes in future precipitation. That means four out of ten tier-I cities will be exposed to hotspots towards EOC, which is quite alarming. The list of these 202 hotspot cities along with their PVI values is provided in Table-S3 of supplementary information. However for brevity in representation, we filtered out 89 cities with population more than 5 lakhs out of total 493 tier-I cities, and identified 41 cities (approximately 46%) among them to be hotspots to precipitation changes. The location of these 89 cities with different coloured markers (Red, orange, yellow and green) is shown in Fig. 12 to distinguish them under different zones of vulnerability. We expect this will serve as a useful piece of information for urban planners and policy makers to plan adequately before facing the challenging future. However, it is worthwhile to mention that, consideration of sub-daily scale precipitation could have been more meaningful for identification of vulnerable cities. However, sub-daily scale analysis is beyond the scope of the current study due to non-availability of reliable data over entire India – both from observation and model-simulations, and therefore, kept as a future scope of the study.

Although the hotspot patterns are apparently robust under different emission scenarios, the results can be subjected to some sources of uncertainty. For example, in spite of using state-of-the-art CMIP6-GCMs, the number of models and realizations used may not be sufficient enough to capture the full range of uncertainty in the perspective of global climate sensitivity and regional response to global warming (Taylor et al., 2012). Thus despite considering MME mean, the final results could be sensitive to the number of models and its realizations considered. Another source of uncertainty can arise from the temporal scale of this analysis, which is multi-decadal here. Hence, the identified precipitation changes patterns could be overwhelmed by the internal climatic variability for shorter time scales such as, decadal or sub-decadal periods. Moreover, the assumption of stationary bias in the data is another limitation of the approach. In general, most of the existing bias-correction methods including RMPH method inherently assume stationarity in the bias, which questions the model applicability in the future, particularly in the far-future period. Notwithstanding, the overall findings of this study cannot be denied for adopting better preparedness and informed policy formulation for future.

## 5. Conclusions

This study proposes a new and more inclusive index named Precipitation based Hotspot Index (PHI) to identify the ‘hotspots’ across the Indian mainland considering the most expected changes in the precipitation pattern in the future. Future simulated precipitation data from 14 state-of-the-art GCMs, participating in CMIP6, under two possible climate change scenarios – SSP245 and SSP585 have been utilised for this purpose. The raw GCM data is properly bias-corrected using a latest

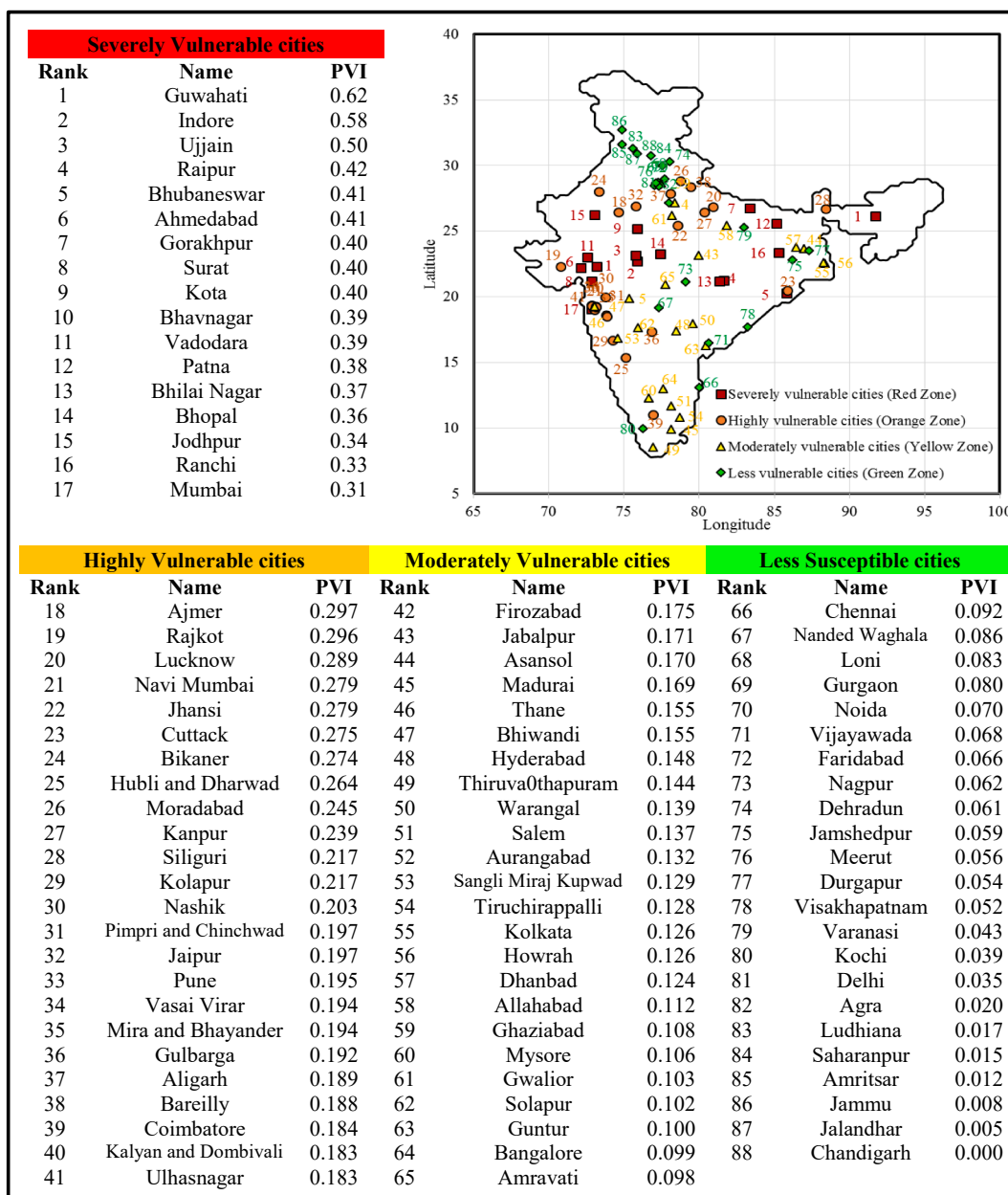


Fig. 12. Name and location of all 88 cities with more than 5 lakh population in India and their categorisation into four vulnerability groups, red, orange, yellow and green. The red and orange marked cities are considered as precipitation change vulnerable cities in this study. (For interpretation of the references to color in this figure legend, the reader is referred to the web version of this article.)

copula-based technique (i.e., RMPH method) and made available in public domain (<https://figshare.com/s/9d978fcff33e86bbf56b>). Next, an analysis of this bias-corrected future precipitation is carried out at various temporal as well as spatial scales to understand the underlying mechanisms of these hotspot regions. Finally, all the cities (a total of 493) across the country with more than 1 lakh population are considered to identify the most vulnerable cities in India. Overall the key observations of this study are listed below.

1. In general, a wetter climate is projected across Indian mainland with approximately  $290 \pm 150$  mm to  $530 \pm 260$  mm increase in annual precipitation towards the end of this century under various models and scenarios. The increase is persistent over the future years and gets more intense with time, particularly under the higher emission scenario- indicating a potential impact of increased anthropogenic activities on the extreme precipitation.

2. This increase in annual precipitation has considerable spatio-temporal variations considering different seasons and HPZs. Season-wise, the summer and monsoon precipitation contributes the most towards the total increase in annual precipitation, whereas the post-monsoon shows a relatively weaker level of increase, and winter precipitation shows an overall decline. Thus, the wet months are projected to be wetter and dry months will remain mostly the same or even may get drier. Spatially, the low-precipitation zones (HPZ-1 and HPZ-4) show the maximum increase (in percentage), whereas the high-precipitation zones like HPZ-6 shows the least increase.

3. The increase is projected in both the levels of precipitation-mean and extremes. However, the increase (in percentage) is more in case extremes than the mean level. For instance, the increase in AMDP (~45%) towards the end of the century is almost two-fold than the increase in precipitation median (~23%) following SSP585. As expected, such an alarming level of increase in extreme precipitation is

likely to have detrimental impacts on various socio-economic sectors of the country.

- Based on these future projected changes in various aspects of precipitation, such as mean, variability, and extremes (magnitude, frequency and intensity), the PHI is evaluated and accordingly entire Indian mainland is categorised into four susceptibility zones -red, orange, yellow, and green. Out of these four color-coded regions, the red and orange colored zones together are identified as hotspot regions, which are projected to have high to severe changes in precipitation towards the end of century under SSP585 scenario. These hotspot regions mostly spans in northwest, west-central, west-coast, northeast and some sub-Himalayan regions in India.
- Zone-wise analysis reveals that HPZ-1 and HPZ-6 are most extensively occupied by the hotspot region as compared to other HPZs. Almost three-fourth of the areal extent of HPZ-1 and HPZ-6 are exposed to high to severe changes in precipitation. On the other hand, moderate precipitation zones (e.g., HPZ-2 and HPZ-5) are projected to face the lowest areal extent exhibiting changes in precipitation.
- Finally, considering two important socio-economic factors viz., population density (PD) and human development index (HDI) along with the PHI, another index named Precipitation-based Vulnerability Index (PVI) is defined. Based on that, the key-vulnerable tier-I cities are identified across India. The analysis with 493 Indian cities with more than 1 lakh population reveals four out of ten tier-I cities will be exposed to high vulnerability towards the end of this century.

Overall, the findings of this study on future-projected changes in precipitation over India is expected to be beneficial for management of water resources considering in future change. Such an extent of rise of various levels of precipitation will pose multi-dimensional challenges. Hence, suitable adaptation and mitigation strategies are required to be formulated in advance to build resilience against the worst-case climate change scenario. The precipitation-based hotspot map along with identified vulnerable cities within various susceptibility zones may be helpful for the urban planners and decision-makers to formulate suitable strategies and for sustainable planning and development in future.

#### Declaration of Competing Interest

The authors declare that they have no known competing financial interests or personal relationships that could have appeared to influence the work reported in this paper.

#### Data availability

Data will be made available on request.

#### Acknowledgements

This study is supported by a sponsored project supported by Ministry of Earth Science (MoES), Govt. of India, through a sponsored project (Grant no. MoES/PAMC/H&C/124/2019-PC-II). Authors further acknowledge the National Supercomputing Mission (NSM) for providing computing resources of 'PARAM Shakti' at IIT Kharagpur, which is implemented by C-DAC and supported by the Ministry of Electronics and Information Technology (MeitY) and Department of Science and Technology (DST), Government of India. Finally, the authors thank the editors and two anonymous reviewers whose constructive comments immensely improved the manuscript.

#### Appendix A. Supplementary data

Supplementary data to this article can be found online at <https://doi.org/10.1016/j.jhydrol.2023.129805>.

#### References

- Ashfaq, M., Rastogi, D., Mei, R., Touma, D., Ruby Leung, L., 2017. Sources of errors in the simulation of south Asian summer monsoon in the CMIP5 GCMs. *Clim. Dyn.* 49, 193–223. <https://doi.org/10.1007/s00382-016-3337-7>.
- Barbero, R., Fowler, H.J., Lenderink, G., Blenkinsop, S., 2017. Is the intensification of precipitation extremes with global warming better detected at hourly than daily resolutions? *Geophys. Res. Lett.* 44, 974–983. <https://doi.org/10.1002/2016GL071917>.
- Chen, C.A., Hsu, H.H., Liang, H.C., 2021. Evaluation and comparison of CMIP6 and CMIP5 model performance in simulating the seasonal extreme precipitation in the Western North Pacific and East Asia. *Weather Clim. Extrem.* 31, 100303 <https://doi.org/10.1016/j.wace.2021.100303>.
- Costello, A., Abbas, M., Allen, A., Ball, S., Bell, S., Bellamy, R., Friel, S., Groce, N., Johnson, A., Kett, M., Lee, M., Levy, C., Maslin, M., McCoy, D., McGuire, B., Montgomery, H., Napier, D., Pagel, C., Patel, J., de Oliveira, J.A.P., Redclift, N., Rees, H., Rogger, D., Scott, J., Stephenson, J., Twigg, J., Wolff, J., Patterson, C., 2009. Managing the health effects of climate change. *Lancet and University College London Institute for Global Health Commission. Lancet* 373, 1693–1733. [https://doi.org/10.1016/S0140-6736\(09\)60935-1](https://doi.org/10.1016/S0140-6736(09)60935-1).
- Dash, S., Maity, R., 2019. Temporal evolution of precipitation-based climate change indices across India : contrast between pre- and post-1975 features. *Theor. Appl. Climatol.*
- de Sherbinin, A., 2014. Climate change hotspots mapping: What have we learned? *Clim. Change* 123, 23–37. <https://doi.org/10.1007/s10584-013-0900-7>.
- De Souza, K., Kituyi, E., Harvey, B., Leone, M., Murali, K.S., Ford, J.D., 2015. Vulnerability to climate change in three hot spots in Africa and Asia: key issues for policy-relevant adaptation and resilience-building research. *Reg. Environ. Chang.* 15, 747–753. <https://doi.org/10.1007/s10113-015-0755-8>.
- Di Luca, A., Pitman, A.J., de Elia, R., 2020. Decomposing Temperature Extremes Errors in CMIP5 and CMIP6 Models. *Geophys. Res. Lett.* 47, 1–10. <https://doi.org/10.1029/2020GL088031>.
- Diffenbaugh, N.S., Giorgi, F., 2012. Climate change hotspots in the CMIP5 global climate model ensemble. *Clim. Change* 114, 813–822. <https://doi.org/10.1007/s10584-012-0570-x>.
- Eyring, V., Bony, S., Meehl, G.A., Senior, C.A., Stevens, B., Stouffer, R.J., Taylor, K.E., 2016. Overview of the Coupled Model Intercomparison Project Phase 6 (CMIP6) experimental design and organization. *Geosci. Model Dev.* 9 (5), 1937–1958.
- Flato, G., Marotzke, J., Abiodun, B., Braconnot, P., Chou, S.C., Collins, W., Cox, P., Driouech, F., Emori, S., Eyring, V., Forest, C., Gleckler, P., Guilyardi, E., Jakob, C., Kattsov, V., Reason, C., Rummukainen, M., 2013. Evaluation of climate models, *Climate Change 2013 The Physical Science Basis: Working Group I Contribution to the Fifth Assessment Report of the Intergovernmental Panel on Climate Change*. Cambridge University Press, Cambridge, United Kingdom and New York, NY, USA. <https://doi.org/10.1017/CBO9781107415324.020>.
- Gidden, M.J., Riahi, K., Smith, S.J., Fujimori, S., Luderer, G., Kriegler, E., Van Vuuren, D. P., Van Den Berg, M., Feng, L., Klein, D., Calvin, K., Doelman, J.C., Frank, S., Fricko, O., Harmsen, M., Hasegawa, T., Havlik, P., Hilaire, J., Hoesly, R., Horing, J., Popp, A., Stehfest, E., Takahashi, K., 2019. Global emissions pathways under different socioeconomic scenarios for use in CMIP6: A dataset of harmonized emissions trajectories through the end of the century. *Geosci. Model Dev.* 12, 1443–1475. <https://doi.org/10.5194/gmd-12-1443-2019>.
- Giorgi, F., 2006. Climate change hot-spots. *Geophys. Res. Lett.* 33, 1–4. <https://doi.org/10.1029/2006GL025734>.
- Guhathakurta, P., Sreejith, O.P., Menon, P.A., 2011. Impact of climate change on extreme rainfall events and flood risk in India. *J. Earth Syst. Sci.* 120 (3), 359–373.
- Ionescu, C., Klein, R.J.T., Hinkel, J., Kavi Kumar, K.S., Klein, R., 2009. Towards a formal framework of vulnerability to climate change. *Environ. Model. Assess.* 14, 1–16. <https://doi.org/10.1007/s10666-008-9179-x>.
- Jones, B., O'Neill, B.C., 2016. Spatially explicit global population scenarios consistent with the Shared Socioeconomic Pathways. *Environ. Res. Lett.* 11 (8), 084003.
- Kishore, P., Jyothi, S., Basha, G., Rao, S.V.B., Rajeevan, M., Velicogna, I., Sutterley, T.C., 2015. Precipitation climatology over India: validation with observations and reanalysis datasets and spatial trends. *Clim. Dyn.* 46, 541–556. <https://doi.org/10.1007/s00382-015-2597-y>.
- Knutti, R., Rogelj, J., Sedláček, J., Fischer, E.M., 2016. A scientific critique of the two-degree climate change target. *Nat. Geosci.* 9, 13–18. <https://doi.org/10.1038/ngeo2595>.
- Kothawale, D.R., Rajeevan, M., 2017. Monthly, Seasonal and Annual Rainfall Time Series for All-India, Homogeneous Regions and Meteorological Subdivisions : 1871–2016. *Indian Inst. Trop. Meteorol. Earth Syst. Sci. Organ. Minist. Earth Sci.* 02, 1–164.
- Kumm, M., Taka, M., Guillaume, J.H.A., 2018. Gridded global datasets for Gross Domestic Product and Human Development Index over 1990–2015. *Sci. Data* 5, 1–15. <https://doi.org/10.1038/sdata.2018.4>.
- Kusumastuti, C., Jiang, Z., Mehrotra, R., Sharma, A., 2021. A Signal Processing Approach to Correct Systematic Bias in Trend and Variability in Climate Model Simulations. *Geophys. Res. Lett.* 48, 1–11. <https://doi.org/10.1029/2021GL092953>.
- Leander, R., Buishand, T.A., 2007. Resampling of regional climate model output for the simulation of extreme river flows. *J. Hydrol.* 332, 487–496. <https://doi.org/10.1016/j.jhydrol.2006.08.006>.
- Leander, R., Buishand, T.A., van den Hurk, B.J.J.M., de Wit, M.J.M., 2008. Estimated changes in flood quantiles of the river Meuse from resampling of regional climate model output. *J. Hydrol.* 351, 331–343. <https://doi.org/10.1016/j.jhydrol.2007.12.020>.

- Lenderink, G., Buishand, A., Van Deursen, W., 2007. Estimates of future discharges of the river Rhine using two scenario methodologies: Direct versus delta approach. *Hydrol. Earth Syst. Sci.* 11, 1145–1159. <https://doi.org/10.5194/hess-11-1145-2007>.
- Li, J., Huo, R., Chen, H., Zhao, Y., Zhao, T., 2021. Comparative Assessment and Future Prediction Using CMIP6 and CMIP5 for Annual Precipitation and Extreme Precipitation Simulation. *Front. Earth Sci.* 9, 1–20. <https://doi.org/10.3389/feart.2021.687976>.
- Li, H., Sheffield, J., Wood, E.F., 2010. Bias correction of monthly precipitation and temperature fields from Intergovernmental Panel on Climate Change AR4 models using equidistant quantile matching. *J. Geophys. Res. Atmos.* 115 <https://doi.org/10.1029/2009JD012882>.
- Madakumbura, G.D., Kim, H., Utsumi, N., Shioyama, H., Fischer, E.M., Seland, Ø., Scinocca, J.F., Mitchell, D.M., 2019. Event-to-event intensification of the hydrologic cycle from 1.5 °C to a 2 °C warmer world. *Sci. Rep.* 9: 3483, 1–7. <https://doi.org/10.1038/s41598-019-39936-2>.
- Maity, R., Suman, M., Laux, P., Kunstmann, H., 2019. Bias Correction of Zero-Inflated RCM Precipitation Fields : A Copula-Based Scheme for Both Mean and Extreme Conditions. *J. Hydrometeorol.* 595–611 <https://doi.org/10.1175/JHM-D-18-0126.1>.
- Mallya, G., Mishra, V., Niyogi, D., Tripathi, S., Govindaraju, R.S., 2016. Trends and variability of droughts over the Indian monsoon region. *Weather Clim. Extrem.* 12, 43–68. <https://doi.org/10.1016/j.wace.2016.01.002>.
- Mani, M., Bandyopadhyay, S., Chonabayashi, S., Markandya, A., Mosier, T., 2018. South Asia's Hotspots and Precipitations: The Impact of Temperature and Precipitation Changes on Living Standards. South Asia Development Matters, Washington, DC: World Bank. <https://doi.org/10.1596/978-1-4648-1155-5>.
- Mao, G., Vogl, S., Laux, P., Wagner, S., Kunstmann, H., 2015. Stochastic bias correction of dynamically downscaled precipitation fields for Germany through Copula-based integration of gridded observation data. *Hydrol. Earth Syst. Sci.* 19, 1787–1806. <https://doi.org/10.5194/hess-19-1787-2015>.
- Maraun, D., 2013. Bias correction, quantile mapping, and downscaling: Revisiting the inflation issue. *J. Clim.* 26, 2137–2143. <https://doi.org/10.1175/JCLI-D-12-00821.1>.
- Maurer, E.P., Hidalgo, H.G., Das, T., Dettinger, M.D., Cayan, D.R., 2010. The utility of daily large-scale climate data in the assessment of climate change impacts on daily streamflow in California. *Hydrol. Earth Syst. Sci.* 14, 1125–1138. <https://doi.org/10.5194/hess-14-1125-2010>.
- Mehrotra, R., Sharma, A., 2016. A multivariate quantile-matching bias correction approach with auto- and cross-dependence across multiple time scales: implications for downscaling. *J. Clim.* 29, 3519–3539. <https://doi.org/10.1175/JCLI-D-15-0356.1>.
- Mehrotra, R., Sharma, A., 2019. A Resampling Approach for Correcting Systematic Spatiotemporal Biases for Multiple Variables in a Changing Climate. *Water Resour. Res.* 55, 754–770. <https://doi.org/10.1029/2018WR023270>.
- Mehrotra, R., Sharma, A., 2021. A robust alternative for correcting systematic biases in multi-variable climate model simulations. *Environ. Model. Softw.* 139, 105019 <https://doi.org/10.1016/j.envsoft.2021.105019>.
- Mishra, V., Kumar, D., Ganguly, A.R., Sanjay, J., Mujumdar, M., Krishnan, R., Shah, R.D., 2014. Reliability of regional and global climate models to simulate precipitation extremes over India. *J. Geophys. Res. Atmos.* 119, 9301–9323. <https://doi.org/10.1002/2014JD021636>.
- Mishra, V., Bhatia, U., Tiwari, A.D., 2020. Bias-corrected climate projections for South Asia from Coupled Model Intercomparison Project-6. *Sci. Data* 7, 1–10. <https://doi.org/10.1038/s41597-020-00681-1>.
- Mukherjee, S., Aadhar, S., Stone, D., Mishra, V., 2018. Increase in extreme precipitation events under anthropogenic warming in India. *Weather Clim. Extrem.* 20, 45–53. <https://doi.org/10.1016/j.wace.2018.03.005>.
- Niranjan Kumar, K., Rajeevan, M., Pai, D.S., Srivastava, A.K., Preethi, B., 2013. On the observed variability of monsoon droughts over India. *Weather Clim. Extrem.* 1, 42–50. <https://doi.org/10.1016/j.wace.2013.07.006>.
- Pai, D.S., Sridhar, L., Rajeevan, M., Sreejith, O.P., Satbhai, N.S., Mukhopadhyay, B., 2014. Development of a new high spatial resolution (0.25° × 0.25°) long period (1901–2010) daily gridded rainfall data set over India and its comparison with existing data sets over the region. *Mausam* 65, 1–18.
- Pall, P., Aina, T., Stone, D.A., Stott, P.A., Nozawa, T., Hilberts, A.G.J., Lohmann, D., Allen, M.R., 2011. Anthropogenic greenhouse gas contribution to flood risk in England and Wales in autumn 2000. *Nature* 470, 382–385. <https://doi.org/10.1038/nature09762>.
- Parry, M.L., Canziani, O.F., Palutikof, J.P., Linden, P.J. van der, Hanson, C.E., 2007. IPCC, 2007: Climate Change 2007: Impacts, Adaptation and Vulnerability. Contribution of Working Group II to the Fourth Assessment Report of the Intergovernmental Panel on Climate Change, Cambridge University Press, Cambridge, UK. <https://doi.org/10.1016/B978-008044910-4.00250-9>.
- Piani, C., Haerter, J.O., Coppola, E., 2010. Statistical bias correction for daily precipitation in regional climate models over Europe. *Theor. Appl. Climatol.* 99, 187–192. <https://doi.org/10.1007/s00704-009-0134-9>.
- Pierce, D.W., Cayan, D.R., Maurer, E.P., Abatzoglou, J.T., Hegewisch, K.C., 2015. Improved bias correction techniques for hydrological simulations of climate change. *J. Hydrometeorol.* 16, 2421–2442. <https://doi.org/10.1175/JHM-D-14-0236.1>.
- Rajeevan, M., Bhatia, J., Jaswal, A.K., 2008. Analysis of variability and trends of extreme rainfall events over India using 104 years of gridded daily rainfall data. *Geophys. Res. Lett.* 35, 1–6. <https://doi.org/10.1029/2008GL035143>.
- Roe, S., Streck, C., Obersteiner, M., Frank, S., Griscorn, B., Drouet, L., Fricko, O., Gusti, M., Harris, N., Hasegawa, T., Hausfather, Z., Havlík, P., House, J., Nabuurs, G. J., Popp, A., Sánchez, M.J.S., Sanderman, J., Smith, P., Stehfest, E., Lawrence, D., 2019. Contribution of the land sector to a 1.5 °C world. *Nat. Clim. Chang.* 9, 817–828. <https://doi.org/10.1038/s41558-019-0591-9>.
- Rogelj, J., Den Elzen, M., Höhne, N., Fransen, T., Fekete, H., Winkler, H., Schaeffer, R., Sha, F., Riahi, K., Meinshausen, M., 2016. Paris Agreement climate proposals need a boost to keep warming well below 2 °C. *Nature* 534, 631–639. <https://doi.org/10.1038/nature18307>.
- Sarkar, S., Maity, R., 2020a. Increase in Probable Maximum Precipitation in a Changing Climate over India. *J. Hydrol.* 585, 124806 <https://doi.org/10.1016/j.jhydrol.2020.124806>.
- Sarkar, S., Maity, R., 2020b. Estimation of Probable Maximum Precipitation in the context of climate change. *MethodsX* 7, 1–8. <https://doi.org/10.1016/j.mex.2020.100904>.
- Sarkar, S., Maity, R., 2021. Global climate shift in 1970s causes a significant worldwide increase in precipitation extremes. *Sci. Rep.* 11, 1–12. <https://doi.org/10.1038/s41598-021-90854-8>.
- Sarkar, S., Maity, R., 2022. Future Characteristics of Extreme Precipitation Indicate the Dominance of Frequency Over Intensity: A Multi-Model Assessment From CMIP6 Across India. *J. Geophys. Res. Atmos.* 127, 1–22. <https://doi.org/10.1029/2021jd035539>.
- Sen, P.K., 1968. Estimates of the Regression Coefficient Based on Kendall's Tau. *J. Am. Stat. Assoc.* 63, 1379–1389. <https://doi.org/10.1080/01621459.1968.10480934>.
- Sharma, S., Mujumdar, P., 2017. Increasing frequency and spatial extent of concurrent meteorological droughts and heatwaves in India. *Sci. Rep.* 7, 1–9. <https://doi.org/10.1038/s41598-017-15896-3>.
- Stocker, T.F., Qin, D., Plattner, G.K., Tignor, M.M.B., Allen, S.K., Boschung, J., Nauels, A., Xia, Y., Bex, V., Midgley, P.M., 2013. Climate change IPCC 2013 the physical science basis: Working Group I contribution to the fifth assessment report of the intergovernmental panel on climate change. Cambridge University Press, Cambridge, United Kingdom and New York, NY, USA. <https://doi.org/10.1017/CBO9781107415324>.
- Suman, M., Maity, R., 2021. Assessment of basin-wise future agricultural drought status across India under changing climate. *J. Water Clim. Chang.* 12, 2400–2421. <https://doi.org/10.2166/wcc.2021.369>.
- Suman, M., Maity, R., Kunstmann, H., 2022. Precipitation of Mainland India: Copula-based bias-corrected daily CORDEX climate data for both mean and extreme values. *Geosci. Data J.* 9 (1), 58–73.
- Supharatid, S., Nafung, J., Aribarg, T., 2022. Projected changes in temperature and precipitation over mainland Southeast Asia by CMIP6 models. *J. Water Clim. Chang.* 13 (1), 337–356.
- Taylor, K.E., Stouffer, R.J., Meehl, G.A., 2012. An overview of CMIP5 and the experiment design. *Bull. Am. Meteorol. Soc.* 93, 485–498. <https://doi.org/10.1175/BAMS-D-11-00094.1>.
- Themebl, M.J., Gobiet, A., Leuprecht, A., 2011. Empirical-statistical downscaling and error correction of daily precipitation from regional climate models. *Int. J. Climatol.* 31, 1530–1544. <https://doi.org/10.1002/joc.2168>.
- Torres, R.R., Lapola, D.M., Marengo, J.A., Lombardo, M.A., 2012. Socio-climatic hotspots in Brazil. *Clim. Change* 115, 597–609. <https://doi.org/10.1007/s10584-012-0461-1>.
- Trenberth, K.E., Dai, A., Rasmussen, R.M., Parsons, D.B., 2003. The changing character of precipitation. *Bull. Amer. Meteorol. Soc.* 84, 1205–1217. <https://doi.org/10.1175/BAMS-84-9-1205>.
- Turco, M., Palazzi, E., Von Hardenberg, J., Provenzale, A., 2015. Observed climate change hotspots. *Geophys. Res. Lett.* 42, 3521–3528. <https://doi.org/10.1002/2015GL063891>.
- UNFCCC, 2015. Adoption of the Paris Agreement FCCC/CP/2015/L.9/Rev.1, United Nations Framework Convention on Climate Change. Paris, 30 November to 11 December 2015.
- Vrac, M., Friederichs, P., 2015. Multivariate-intervariable, spatial, and temporal-bias correction. *J. Clim.* 28, 218–237. <https://doi.org/10.1175/JCLI-D-14-00059.1>.
- Wang, D., Liu, J., Shao, W., Mei, C., Su, X., Wang, H., 2021. Comparison of cmip5 and cmip6 multi-model ensemble for precipitation downscaling results and observational data: The case of hanjiang river basin. *Atmosphere (Basel)* 12 (7), 867.